OET | Opto-Electronic Technology
www.oejournal.org/oet

Review
September 2025, Vol. 1, No. 2

DOI: 10.29026/oet.2025.250003 | CSTR: 32419.14.oet.2025.250003

Open Access

Femtosecond laser micro/nano-processing via multiple pulses incubation

Jingbo Yin[1,2], Zhenyuan Lin[3], Lingfei Ji[3]* and Minghui Hong[1,2,4]*

Abstract: As a flexible and efficient non-contact processing strategy in ambient air, femtosecond laser precision engineering has become an advanced technology for micro/nano-structure fabrication. Femtosecond laser can output ultrashort laser pulses at a very high repetition rate, ensuring higher machining accuracy and improving the machining efficiency. The femtosecond laser manufacturing is mostly processed under multiple pulses irradiation. At a high repetition rate, incubation effect based on the multiple pulses irradiation provides a new theoretical and technical support to realize precision manufacturing. Herein, a systematic review is conducted on the influence of laser repetition rate spanning from kHz to GHz. The physical mechanisms of three incubation modes, namely defects accumulation (kHz), heat accumulation (MHz), and plasma interaction (GHz), are summarized. The latest progress including micro/nano-structuring, nanostructure synthesis, three-dimensional functional structures fabrication and cross-scale precision engineering is explored. Furthermore, the prospect and challenge of the high-repetition-rate femtosecond laser processing in research frontiers and industrial applications are discussed.

Keywords: high-repetition-rate femtosecond laser; multiple pulses Incubation; laser micro/nano-processing

Introduction

Micro/nano-fabrication provides a unique platform to explore new applications in the fields of materials science[1,2], semiconductors[3,4], sensing[5–7] and biomedicine[8]. Since its naissance in the 1990s, femtosecond laser micro/nano-processing has revolutionized the field of precision manufacturing, leveraging its ultrashort pulse duration (10^{-15} s) and ultrahigh peak power (TW level)[9]. This technology enables micron to nanoscale precision through the precise manipulation of laser-material interactions, and has shown its powerful ability in various micro/nano-precision engineering applications[10,11]. Femtosecond laser processing involves the complex interaction between light and matters[12], which is both challenging with opportunity[13]. Based on the special understanding of the laser-materials interactions, two technology categories have been developed, including near-field processing[14] and far-field processing[15]. The near-field processing technology relies on the manipulation and control of attenuated evanescent waves, which has extremely high machining accuracy but limited throughput[16]. The far-field processing technology based on multiphoton absorption[17], threshold effect[18] and incubation[19] have been developed, which greatly improves the potentials of laser micro/nano-engineering. With breakthroughs in laser technology, the femtosecond laser repetition rate has increased from early kHz to current GHz, spanning the six orders of magnitude[20,21]. This evolution leap not only drives exponential improvements in processing efficiency (from thousands to billions of pulses per second) but also produces novel processing methods[22]. In the process of the high-repetition-rate femtosecond laser irradiation, various extreme manufacturing has been realized via multiple pulses incubation[23].

Here, we systematically summarize the influence of femtosecond laser repetition rate (from kHz to GHz) on micro/nano-processing via multiple pulses incubation. The physical mechanisms of three incubation modes: defects accumulation at kHz, heat accumulation at MHz, and plasma interaction at GHz are comprehensively analyzed. By integrating practical applications, the latest progress in femtosecond laser precision engineering based on multiple pulses incubation is emphatically introduced, as depicted in Fig. 1[24–31]. At a repetition rate of kHz, the incubation effect manifests as a reduction in the ablation threshold due to the accumulation of surface defects inside materials. The

Received: 28 May 2025
Accepted: 8 July 2025
Published online: 26 August 2025

[1]Pen-Tung Sah Institute of Micro-Nano Science and Technology, Xiamen University, Xiamen 361005, China; [2]Discipline of Intelligent Instrument and Equipment, Xiamen University, Xiamen 361005, China; [3]School of Physics and Optoelectronic Engineering, Beijing University of Technology, Beijing 100124, China; [4]Innovation Laboratory for Sciences and Technologies of Energy Materials of Fujian Province (IKKEM), Xiamen 361005, China.
*Correspondence: LF Ji, E-mail: ncltji@bjut.edu.cn; MH Hong, E-mail: elehmh@xmu.edu.cn

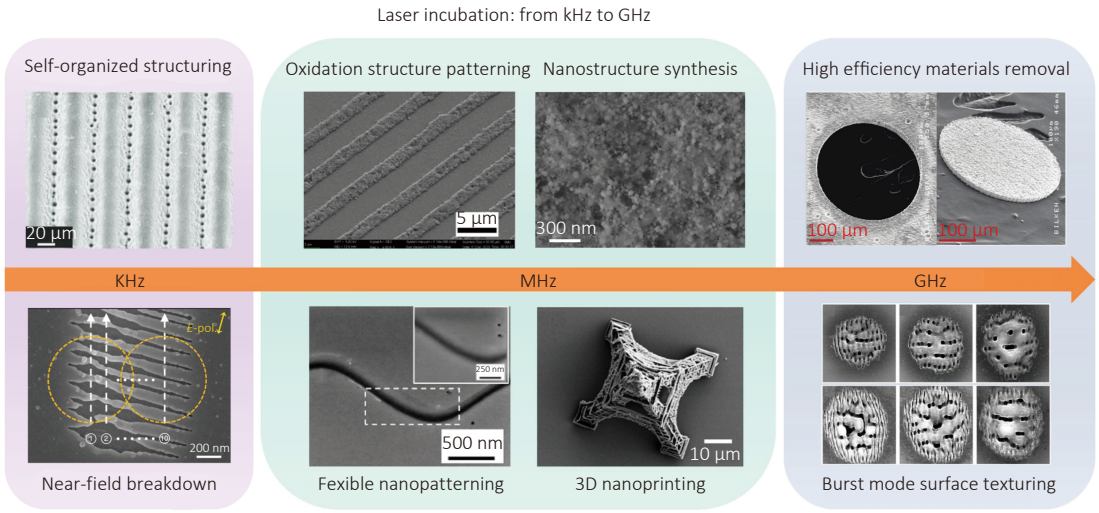

Fig. 1 | Femtosecond laser micro/nano-processing based on multiple pulses incubation. kHz: Self-organized structuring[24] and near-field breakdown[25]; MHz: Oxidation structure patterning[26], nanostructure synthesis[27], flexible nanopatterning[28], and 3D nanoprinting[29]; GHz: High efficiency materials removal[30] and burst mode surface texturing[31].

formation of self-organized structures and near-field breakdown nanostructures is achieved through the defects induced incubation. When the repetition rate reaches MHz, the thermal relaxation time of the materials and the pulse interval achieve a dynamic equilibrium, resulting in the heat accumulation. Through the precise control of this thermal incubation, various processes can be realized, such as oxidation structure patterning, nanostructure synthesis, flexible nanopatterning, and 3D patterning. At a GHz repetition rate, the subsequent pulse can directly interact with the plasma generated by the previous pulse. This interaction significantly enhances energy coupling, leading to the emergence of high efficiency materials removal and burst mode surface texturing. These processing strategies based on multiple pulses incubation provide unique insights for the femtosecond laser precision engineering. Furthermore, the challenges and future prospects of high-repetition-rate femtosecond lasers in both fundamental research frontiers and industrial applications are discussed.

Evolution and incubation mechanism of high-repetition-rate ultrafast laser processing

Since the first ruby laser was invented in 1960[32], laser processing has experienced a revolutionary leap from long pulse (millisecond level) to ultrashort pulse (femtosecond level). Long pulse laser processing is characterized by pronounced thermal diffusion[33], with processing precision constrained by the size of the heat-affected zone (tens of microns), which poses challenges for modern micro/nano-manufacturing. With the breakthrough in chirped-pulse amplification (CPA) technology[34], femtosecond lasers, characterized by their ultrashort pulse duration and ultrahigh peak power, enable the ultimate temporal compression of energy. The light-matters interaction under such extreme conditions has broken the physical limits of traditional thermal processing, enabling cold processing with the minimal heat-affected zone[35]. With the further increase of laser repetition rate, incubation mechanism based on the synergistic effect of multiple pulses irradiation emerges, which further promotes the development of laser precision engineering[30].

Laser-material interaction under different pulse durations and repetition rates

Since the laser processing represents a dynamic and complex process, it is particularly necessary to regulate the interaction between the laser and materials to achieve high-efficiency and high-precision micro/nano-manufacturing. The light-matters interaction encompasses both photothermal and photochemical processes. The photochemical process modifies photosensitive materials through the breaking of chemical bonds that take place upon laser irradiation. This process is applied in photolithography and photo-polymerization for 3D printing[16,36]. In the photothermal process, electrons within the substrate materials upon laser irradiation absorb the energy of incident photons. Subsequently, through intense collisions on a picosecond timescale, the absorbed energy is transferred to the substrate lattice, consequently leading to an increase of substrate surface temperature[37]. As the surface temperature exceeds the melting point or even the boiling point, a phase transition from solid to liquid and then to gas occurs, and a plasma is generated. When the laser irradiation ceases, the substrate undergoes rapid cooling, and ablation craters are formed on the substrate surface.

These processes vary among metals, semiconductors and dielectrics[38]. Metals contain a large number of free electrons, which absorb the energy of incident photons and get

heated up. Via the interaction between electrons and phonons, the heated free electrons transfer energy to the atoms within the lattice. Since semiconductors possess a relatively small number of free electrons, additional electrons are excited across the bandgap. The photon energy of incident light must exceed the band gap of the semiconductors for strong absorption. Electron-hole pairs can be produced by absorbing the energy of incident photon, which corresponds to the interband transition of electrons from the valence band to the conduction band, and causes lattice vibration, thereby heating up the materials. When the density of free electrons is relatively high, the interaction between laser and semiconductors is similar to that of metals. For wide bandgap dielectrics, they are transparent to most of the incident light, and difficult to directly absorb laser energy. The main mechanism of free electrons generated by photons with energy lower than the bandgap involves nonlinear processes like multiphoton ionization. Under a high laser intensity, valence band electrons absorb multiple photons and transition to the conduction band, thereby becoming free electrons. Since this process has a positive correlation with laser peak power, it is more prone to occur during the ultrashort pulse laser processing. In this case, a high concentration of conductive electrons can be generated, which makes the interaction between light and dielectrics similar to metals and semiconductors. Meanwhile, laser machining based on photothermal process involves the heat transfer between electrons and lattice in picosecond time scale, so the machining outcome is highly sensitive to laser pulse duration[39].

For nanosecond laser, due to the long pulse duration, significant thermal effect occurs throughout the process[40,41]. The nanosecond laser processing often results in a large-scale heat-affected zone (HAZ), with its size reaching up to tens of microns. The significant thermal effect also causes the materials to be expelled from the sample surface during the processing, leaving substantial debris around the irradiated area, as shown in Fig. 2(a). For femtosecond laser, with pulse duration $t<10^{-13}$ s, the energy injection occurs at an extremely rapid rate. Thus, the absorbed energy is unable to be transferred from the electrons to the lattice within such a short time interval. The electrons-electrons interaction only increases the local electrons temperature, thus realizing the non-equilibrium state between the electrons and lattice temperature. Since atoms are restricted by their lattice positions, they lack sufficient time to acquire kinetic energy from hot electrons. As a result, the HAZ is small, as depicted in Fig. 2(b). As the injection time of femtosecond laser energy is extremely short, the machining can realize direct solid-vapor or solid-plasma transition, which inhibits thermal diffusion and realizes the laser ablation with smaller HAZ. Moreover, nonlinear absorption during the femtosecond laser processing also limits the focal volume of laser energy deposition and further improves the machining accuracy[42].

When the femtosecond laser outputs laser pulses at a very high repetition rate, it introduces the following mechanisms to further reduce the HAZ. For MHz femtosecond laser, the interval between adjacent pulses is on the order of nanoseconds, which is typically shorter than the thermal relaxation time of lattice cooling (~100 ns)[43]. Therefore, there is heat accumulation between adjacent pulses during the MHz femtosecond laser irradiation, which reduces the laser pulse energy required for the ablation. The precise

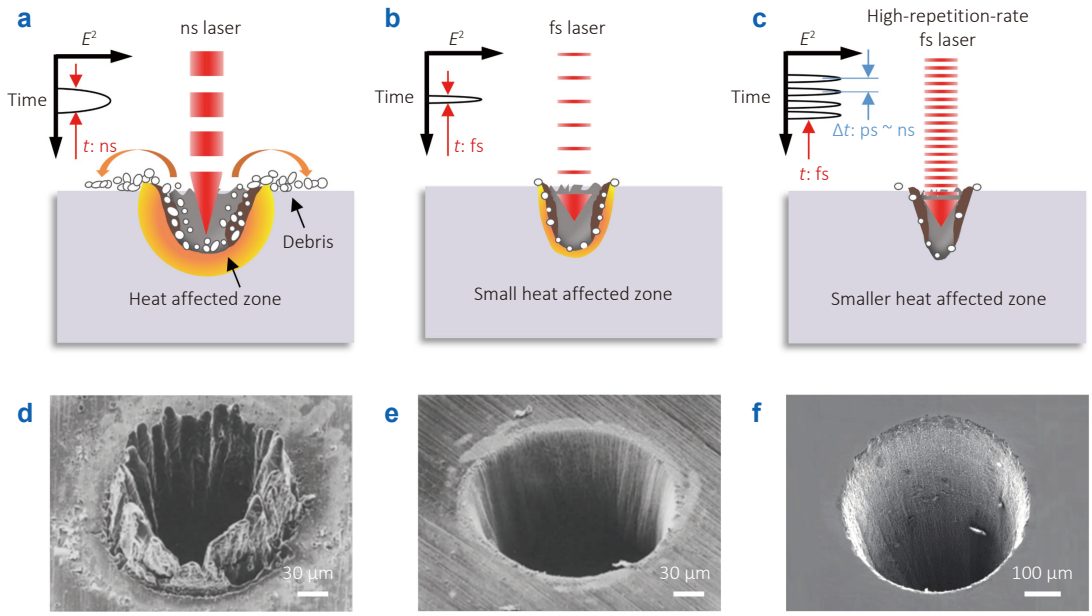

Fig. 2 | Schematic of laser interaction with materials under different pulse durations and repetition rates. (**a**) Nanosecond laser. (**b**) Femtosecond laser. (**c**) High-repetition-rate femtosecond laser. SEM images of laser ablated holes fabricated by (**d**) nanosecond laser[9], (**e**) femtosecond laser[9], and (**f**) high-repetition-rate femtosecond laser[30]. Figure reproduced with permission from: (d, e) ref.[9], (f) ref.[30], Spring Nature.

control of the materials states can be realized under much lower single pulse energy and multiple pulses cumulative irradiation, thus improving the machining accuracy and reducing HAZ[28]. Regarding GHz femtosecond laser, the time interval between adjacent pulses is on the picosecond scale, which is the same as the time scale of lattice heating. In this case, before the residual heat generated by the previous pulse diffuses, the subsequent pulse has already been injected to ablate the materials and carry away the heat, thus achieving "ablation-cooled"[30] and significantly reducing the HAZ. Therefore, the unique mechanism of high-repetition-rate femtosecond laser processing enables precision machining with a much smaller HAZ, as shown in Fig. 2(c). Surface ablation under the irradiation of nanosecond laser, femtosecond laser and high-repetition-rate femtosecond laser are illustrated in Fig. 2(d–f). The ablation of the nanosecond laser processing produces a large HAZ with poor surface quality, as indicated in Fig. 2(d)[9]. The longer pulse duration makes the electrons energy have enough time to conduct into the lattice, resulting in the formation of a larger molten layer, which significantly reduces the machining accuracy. Femtosecond laser irradiation significantly suppresses the HAZ and achieves cold processing. There is basically no molten substance around the laser irradiation area, as shown in Fig. 2(e)[9]. High-repetition-rate femtosecond laser removes heat by ablating materials, thereby further enhancing the processing quality. In Fig. 2(f), the thermal diffusion from the machining region to the surrounding is minimal that enables ablation with an almost negligible HAZ[30].

Incubation effect in femtosecond laser processing

The incubation effect in the laser-material interaction was originally derived from the study of laser-induced surface damage threshold. As early as the 1990s, researchers observed that when materials were subjected to multiple laser pulses irradiation, the materials damage threshold decreases with pulse number[44]. This phenomenon cannot be simply explained by the traditional theory of single pulse laser-material interaction. The origin of the incubation effect can be traced back to the materials sub-damage state induced by the initial laser pulse. Each laser pulse deposits energy into the materials, thus leading to the formation of defects, such as vacancies, interstitials, or dislocations[45,46]. These defects act as nucleation sites for subsequent damages, making the materials more susceptible to laser-induced alterations[47]. Although the initial defects may not be sufficient to cause visible damage to the materials, they gradually accumulate under the multiple pulses irradiation[48]. When the material is exposed to a small number of laser pulses, the defect density is relatively low and the energy required to induce damage is high. However, as more pulses are applied, the defect density increases, leading to a decrease of the energy threshold to induce the damages. This decrease continues until the saturation is reached, at which the accumulation of defects tends to stabilize, thus generating a constant threshold at a large pulse number[49]. Figure 3(a) shows the surface damage thresholds of a-SiO_2 and yttrium lithium fluoride (YLF) plotted in a semi-logarithmic scale with respect to the number of laser irradiations N[44]. For a-SiO_2, after 10 laser pulse irradiations, the surface damage threshold significantly decreases to approximately 1.5 J/cm², which is only 40% of single-pulse irradiation (3.7 J/cm²). After about 100 laser pulse irradiations, the surface damage threshold stabilizes, being approximately 20% of single-pulse irradiation. Meanwhile, the change of damage threshold from ~4.0 to 2.5 J/cm² are also observed in YLF material. In the early

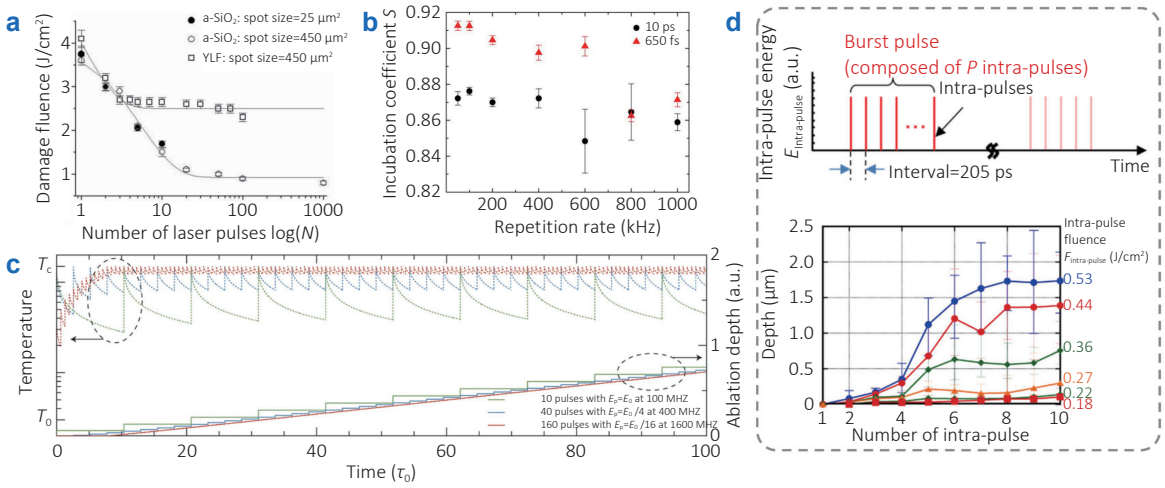

Fig. 3 | (**a**) Dependence of materials surface damage threshold on pulse number. (**b**) Relationship between the incubation coefficient S in laser ablation and the pulse repetition rate. (**c**) Heat accumulation phenomenon of the materials surface during high-repetition-rate femtosecond laser irradiation. (**d**) The pulse form under the GHz burst mode and the dependence of the ablation depth on the number of intra-pulses in the GHz burst pulses[51]. Figure reproduced from: (a) ref.[44], Elsevier; (b) ref.[50], Optical Society of America; (c) ref.[30], Spring Nature; (d) ref.[51], under a Creative Commons Attribution License.

days, the laser repetition rate was relatively low, and the time interval between adjacent pulses was long enough without heat accumulation. The incubation mainly comes from the defects accumulation in the laser-irradiated area.

With the continuous development of laser technology, the repetition rate of femtosecond lasers can range from kHz to GHz, and the time interval between adjacent pulses keeps decreasing. In addition to the incubation caused by the defects accumulation in spatial positions, there is thermal incubation caused by heat accumulation between the adjacent pulses of high-repetition-rate femtosecond laser. Figure 3(b) illustrates the relationship between the incubation coefficient S in laser ablation and repetition rate[50]. When the laser repetition rate is below 600 kHz, the incubation coefficient S of the femtosecond laser at a pulse width of 650 fs shows little variation. However, as laser repetition rate increases above 600 kHz, the incubation coefficient S decreases significantly, indicating a stronger incubation effect. It suggests that at a high laser repetition rate, the heat accumulation is enhanced, thereby promoting the incubation in laser ablation. The calculated evolution of temperature changes on the materials surface under the high-repetition-rate femtosecond laser irradiation is shown in Fig. 3(c)[30]. When the time interval between the adjacent pulses is shorter than the thermal relaxation time of materials cooling, there is a distinct heat accumulation on the materials surface. As the repetition rate increases, the heat accumulation becomes more severe. At this moment, the energy of a single pulse required for the laser ablation is significantly reduced, since the materials can continuously accumulate heat with the increase of pulse irradiation, and ablation can be realized after the accumulation of multiple pulses. By precisely controlling the materials state through the thermal incubation, many novel schemes of laser micro/nano-machining have been achieved.

GHz burst mode femtosecond laser generates pulse trains at a relatively low repetition rate (mostly in kHz range), however, each pulse train contains multiple intra-pulses. The repetition rate within the pulse train can reach up to GHz, and the pulse interval is only a few hundred picoseconds. Figure 3(d) demonstrates the influence of intra-pulses number on the materials ablation depth for the GHz burst mode[51]. When the laser fluence is kept as a constant, with the increase of intra-pulses number, the materials ablation depth is significantly enhanced. When the number of intra-pulses reaches 5, the ablation depth increases sharply, which is due to the interaction between laser pulses and plasma. Laser-induced plasma is usually generated within the picosecond time scale after the laser irradiation and reaches its maximum on the nanosecond scale[52]. Therefore, the following intra-pulses can interact with the plasma generated by the first pulse, thereby increasing the ablation depth. The GHz femtosecond laser based on the burst mode provides the possibility to regulate the interaction of plasmas among adjacent pulses, and also brings about a new mechanism behind the incubation effect.

Therefore, the special understanding based on multiple pulses incubation provides theoretical support to realize new precision manufacturing. Combined with the practical applications of femtosecond laser from kHz to GHz, the latest progress, future prospects and challenges of femtosecond laser precision engineering based on incubation effect will be emphatically introduced.

Incubation effect of kHz femtosecond laser based on defects accumulation

The incubation effect of kHz femtosecond lasers comes from the defects accumulation in the irradiated area. The surface roughness is increased due to the defects accumulation, and then the materials absorption of subsequent laser pulses energy is enhanced. Due to the random location of defects generated, the surface texture produced by multiple pulses incubation also exhibits the feature of irregularity. By optimizing laser processing parameters, including laser fluence, scanning speed, scanning path, scanning time and polarization, the random structure can be adjusted thereby obtaining self-organized structures with certain regularity. In addition, although the defects randomly generated in the laser-irradiated area are uncontrollable, by artificially creating a defect to guide the subsequent multiple pulses incubation, the controllability of the entire process increases, showing excellent application potentials. This section introduces the related applications of self-organized surface structuring and defects-guided near-field breakdown nanostructuring.

Self-organized surface structuring

Functional surface structuring endows materials with a wide range of unique applications[53,54]. Laser surface structuring has proven to be an effective means of altering the surface properties of materials. In addition to conventional laser ablation, multiple pulses laser incubation can also generate unique self-organized surface structures, which have been applied to manufacture various functional surfaces[55]. Xu et al. found that the surface defects in the irradiated area are vital to the excitation of surface plasmon polaritons (SPP) in laser processing[56]. By multiple pulses incubation with pulse energy far below the single-pulse ablation threshold, cross-period surface structures are formed on the silicon surface. Liu et al. proved an attractive phenomenon of the formation of self-organized periodic microhole arrays by exposing aluminum foil to kHz femtosecond laser irradiation[24]. The microhole significantly smaller than the focused laser spot size is generated along the laser scanning path, and a highly ordered microholes array is spontaneously formed after 80 scans, as illustrated in Fig. 4(a). The formation of microholes is considered to have three stages: at first, only slight ablation occurs during laser scanning, which changes the surface roughness. In the

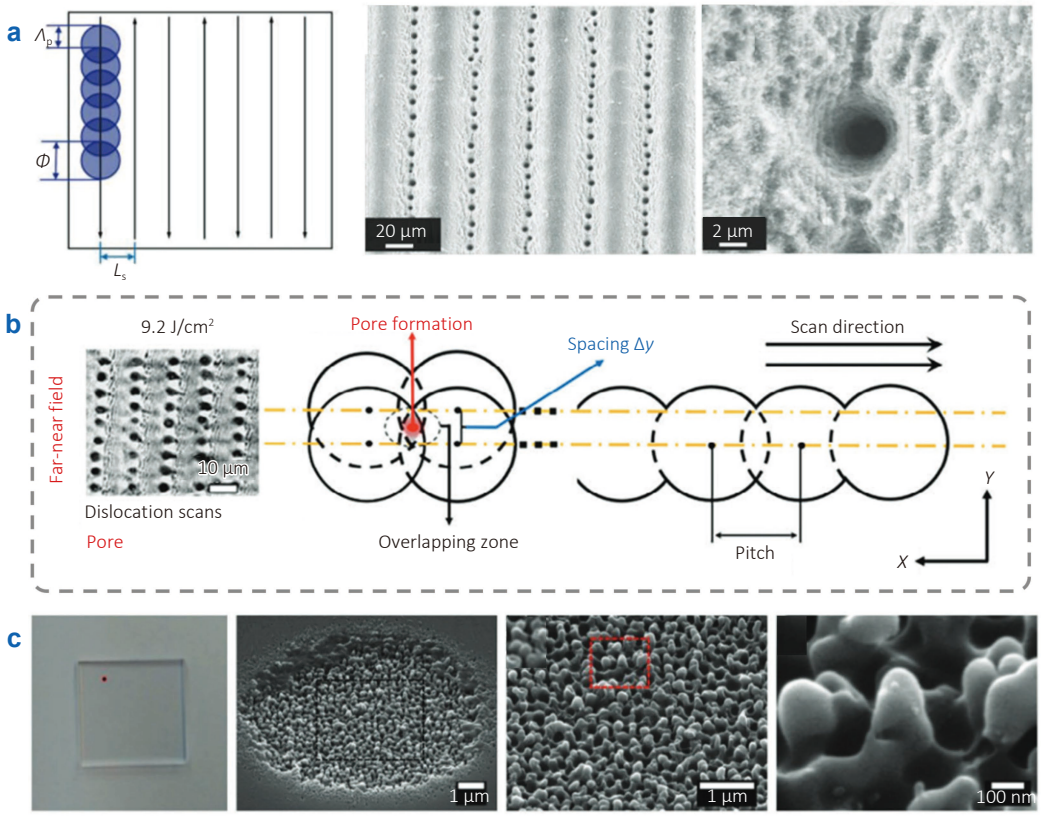

Fig. 4 | (**a**) Periodic microhole arrays formed by self-organized on aluminum surface. (**b**) Self-organized supra-wavelength micro/nano-pores arrays formed on ultra-hard metallic glass (Zr-Cu-Ni-Ti-Al amorphous alloy) by incubation effect. (**c**) Biomimetic nanospike array formed on fused silica glass surface by multiple pulses irradiation of circularly polarized femtosecond laser. Figure reproduced with permission from: (a) ref.[24], (b) ref.[57], (c) ref.[58], John Wiley and Sons.

second stage, microholes are gradually formed on the scanning path, which are significantly smaller than the laser spot diameter, randomly distributed and have no obvious regularity. In the final stage, the microhole period has stabilized, and increasing scanning time deepens and enlarges the microholes. The period and diameter of microholes are highly dependent on laser fluence, and controllable microhole arrays with different periods and diameters are realized by adjusting the laser fluence. This novel laser incubation processing strategy provides a new technical route for surface engineering. Huang et al. developed self-organized "supra-wavelength"[57] micro/nano-pores arrays on ultra-hard metallic glass (Zr-Cu-Ni-Ti-Al amorphous alloy) by controlling the overlapping rate of laser spots through dislocation scanning under high laser fluence, as shown in Fig. 4(b). Supra-wavelength periodic surface structure (SWPSS) is firstly formed on the substrate surface. The SWPSS becomes the seed of the subsequent pulse to enhance the optical near-field laser ablation at the specific site, thus promoting the formation of micro/nano-pores. The whole process is realized under multiple pulses irradiation. To better understand this process, a multi-physical field simulation model including electromagnetic field, temperature field, solid mechanics and fluid dynamics is established. The regularity and uniformity of micro/nano-pores arrays can be improved by optimizing laser processing parameters. The surface of the self-organized micro/nano-pores arrays shows excellent anti-infrared reflection ability. Similar processing is also realized on the surfaces of tungsten and chromium substrates with higher melting points, which shows that this strategy has wide materials applicability.

In addition to scanning path, laser polarization also has a significant impact on the processing results. Zhao et al. found that laser polarization has a remarkable influence on the ablation threshold of carbon fiber reinforced polymer (CFRP)[59]. By choosing an appropriate combination of laser processing parameters and polarization, the effective removal of the resin matrix and carbon fibers in CFRP can be achieved. Papadopoulos et al. prepared biomimetic cicada wing nanostructures on fused silica by multiple pulses laser incubation with circularly polarized femtosecond lasers[58]. The structure is inspired by the unique antireflection characteristics of the wings of *Greta oto* and *Cicada Cretensis*[60,61]. Through the irradiation of 15 laser pulses, an ordered array of biomimetic nanospike array is formed on the substrate, as depicted in Fig. 4(c). The morphology of the nanospikes can be regulated by adjusting laser fluence and pulse number. However, nanospikes cannot be formed under a single-pulse irradiation, which indicates that the

role of multiple pulses incubation is of vital importance. The radius of the nanospikes ranges from 70 nm to 100 nm, and the average height is approximately 224 nm. Compared with the untreated glass substrate, the reflectance of the nanospikes array surface is reduced by 10 times. Transparent hard materials with high hardness, high brittleness, and low light absorption are not only difficult to be fabricated but also often encounter the light transmittance loss during the traditional processing. This antireflection surface preparation strategy shows its application potentials in various glass displays and photoelectric devices.

Under the multiple pulses incubation, laser-induced periodic surface structure (LIPSS) is a more common category[62]. Femtosecond laser is more likely to produce subwavelength nanostructures, which has attracted extensive research attention[63]. The formation of LIPSS involves a large number of physical processes, including surface plasmon wave generation, harmonics wave generation, and hydrodynamic instabilities[64]. Its dynamic formation and self-organized mechanism are complicated, and researchers have put forward different theoretical models and mechanism explanations[65,66]. However, some consensus has been reached that the multiple pulses incubation is important for the formation of LIPSS[67,68]. Lin et al. probed into the alterations in surface morphology and the accumulation of roughness under multiple pulses irradiation[69]. This incubation is regarded as the reason ultimately giving rise to the formation of LIPSS on the surface of Zr-based bulk metallic glasses. Near the material damage threshold, the multiple pulses incubation determines the specific morphology of nano-scale surface structures. As the number of fs laser pulses increases, the surface evolves from a rough state to ordered wrinkles, as shown in Fig. 5(a). Two-dimensional materials have attracted great attention in the fields of semiconductor electronic equipment and bioengineering due to their distinctive physicochemical properties[70,71]. Zou et al.

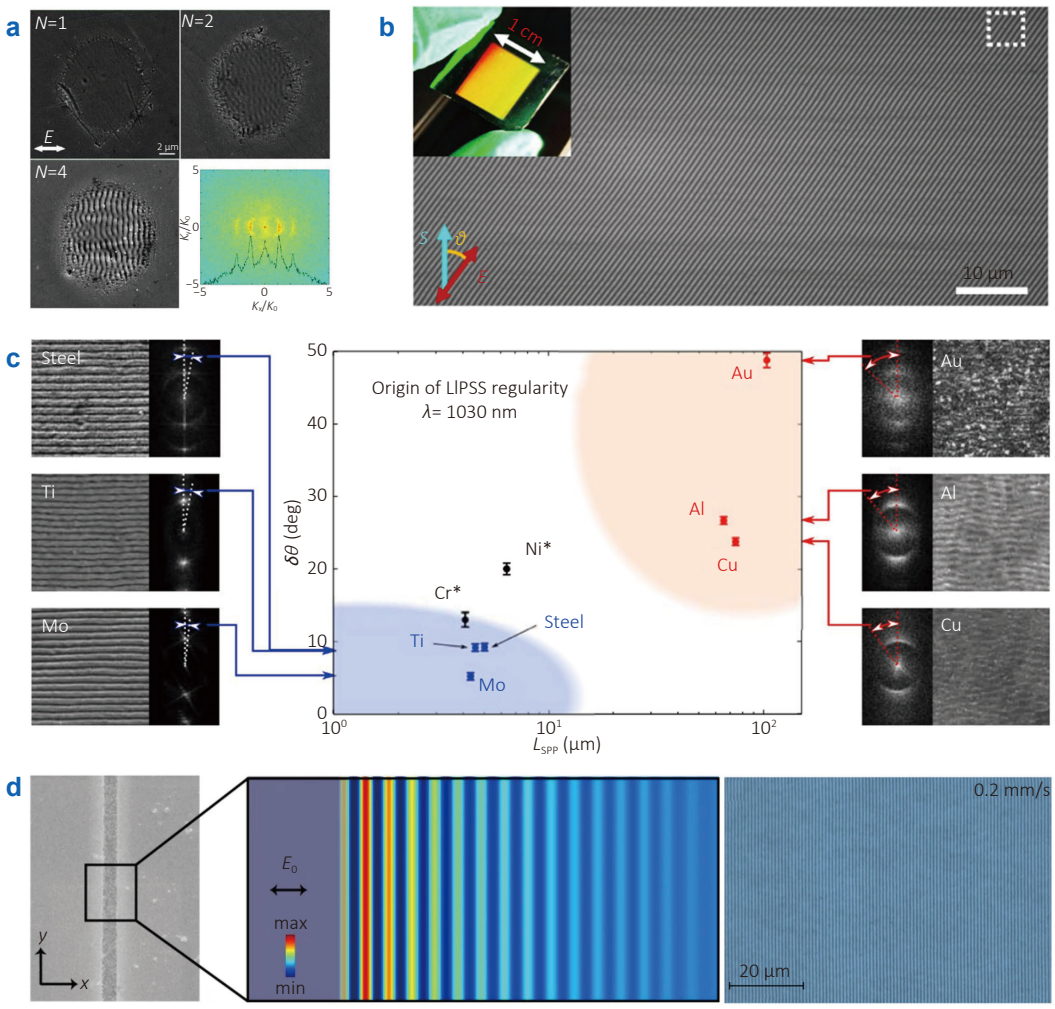

Fig. 5 | (**a**) LIPSS formed on the surface of Zr-based bulk metallic glasses by linearly polarized femtosecond laser irradiation with increasing pulse number. (**b**) Large-area micro/nano-gratings on graphene oxide (GO) films by femtosecond laser irradiation. (**c**) Relationship between LIPSS regularity and decay lengths on different metal surfaces. (**d**) Large-area uniform nanogratings prepared by line-focused femtosecond laser irradiation combined with seed control. Figure reproduced with permission from: (a) ref.[69], (b) ref.[72], (c) ref.[73], (d) ref.[74], under a Creative Commons Attribution License.

prepared large-area micro/nano-gratings on graphene oxide (GO) films by femtosecond laser irradiation[72], as illustrated in Fig. 5(b). The LIPSS formed on the GO films exhibits high robustness to different disturbances. The GO films with highly regular micro/nano-gratings show ~20% enhancement of light absorption in a spectral range of 380–2200 nm. This indicates that the LIPSS strategy can also be extended to the fabrication of nanostructures of two-dimensional materials.

Although LIPSS provides a simple and efficient method to fabricate nanostructures, it faces the challenge of limited controllability. This problem comes from the uneven surface morphology of laser irradiation area, which leads to the difference of multi-physical field in LIPSS dynamic evolution[75]. Meanwhile, different materials and the band perturbations within the materials can also influence the formation of LIPSS[76,77]. Gnilitskyi et al. proposed a calculation method for the surface plasmon polariton decay length (L_{spp}) of different metals[73]. They derived a material-dependent criterion to obtain highly regular LIPSS. By correlating the excited surface electromagnetic waves with L_{spp}, the mechanism behind controlling the regularity of LIPSS was proposed. Specifically, the shorter the decay length of the electromagnetic wave, the more regular the LIPSS is. As depicted in Fig. 5(c), steel, Ti, and Mo exhibit highly regular LIPSS on their surfaces due to smaller L_{spp}. Besides the inherent properties of materials, some researchers have created seed structures within the laser-irradiated area[78,79]. By regulating SPP through these seeds, they can control the morphology of LIPSS. Geng et al. demonstrated a one-step high-throughput uniform nanogratings preparation strategy by line-focused femtosecond laser irradiation combined with seed control[74]. A slit is prepared by laser ablation at the starting point of the LIPSS. This slit acts as a seed, emits SPPs, and generates parallel standing waves through laser-SPPs interference to regulate the growth of LIPSS, as depicted in Fig. 5(d). Cao et al. fabricated large-area subwavelength nanogratings on silicon wafers via direct writing with two-beam interference focused with cylindrical lenses[80]. By adjusting the spacing of interference fringes, coherent resonance enhancement was excited to achieve highly uniform surface plasmon polaritons, thus effectively regulating the growth of LIPSS. Using laser multiple pulses incubation to realize the self-organized structuring provides new insights for various surface engineering. However, further improving structural controllability and realizing more flexible patterns are the focus of this strategy.

Defect-guided nanostructuring

Laser direct writing provides higher flexibility in surface patterning than the self-organized structuring. As introduced in Section *Self-organized surface structuring*, the final morphology of LIPSS can be adjusted by artificial slits. Similarly, the laser direct writing can also be effectively controlled by artificial defects at the starting point of the scanning path. Liu et al. realized nanogroove direct writing with a width less than 40 nm on the ZnO crystal surface by a water immersion objective[81], as shown in Fig. 6(a). They observed the local SPP enhancement in the perpendicular laser polarization direction, thus realizing laser nanostructuring along this direction. Due to the defect at the scanning starting point, the materials ablation threshold is significantly reduced, and the nanogroove width is only 1/20 of the laser wavelength under the multiple pulses incubation. The irradiation pulse number also has a great influence on the nanogrooves formation. With the increase of pulse number, the nanogroove width decreases significantly. The nanogroove is considered to be caused by non-thermal ablation realized by huge local field enhancement under multiple pulses irradiation[82]. Li et al. reported an optical far-field induced near-field breakdown (O-FIB) strategy, which achieved sub-20 nm spatial resolution[25]. They first used multiphoton absorption to create nanopore defects on titanium oxide films as seeds for subsequent multiple pulses incubation. The electric field at the nanopore edge is affected by laser polarization, which shows the enhancement along perpendicular polarization direction and the weakening of parallel direction. Under the guidance of the seeds, scanning along the electric field enhancement direction can realize nanostructuring, as illustrated in Fig. 6(b). Since the electric field enhancement direction is polarization-sensitive, polarization control during the processing is of crucial importance. By adjusting the laser polarization in real time to keep the polarization direction perpendicular to the scanning trajectory defined by the predesigned pattern, curved scanning can be achieved.

This defect-guided nanostructuring strategy based on multiple pulses incubation can also be extended to transparent materials. Li et al. proposed a back-scattering interference crawling mechanism, which realized the cutting width of transparent materials in the range of tens of nanometers with the aspect ratio exceeding 1000[83]. The interference between the incident light and the light backscattered by nanoseeds leads to the cascade generation of the secondary seeds. The near-field enhancement perpendicular to the laser polarization direction promotes the elongation, connection, and uniformization of the seeds, thus generating a crawling effect, as shown in Fig. 6(c). Under multiple pulses irradiation, new seeds are continuously generated, and finally the seeds are continuously connected and extended over the entire focal depth. Combined with chemical etching, the nanodicing of various transparent materials can be realized. Based on the optimized laser processing parameters, the silica nanogratings at a period of 300 nm were prepared, as shown in Fig. 6(d). Defect-guided nanostructuring has provided a new theoretical foundation for various extreme manufacturing processes and also offered new insights into femtosecond laser precision engineering. Currently, this strategy shows a high degree of polarization-dependence. In the future, it is necessary to explore polarization-independent

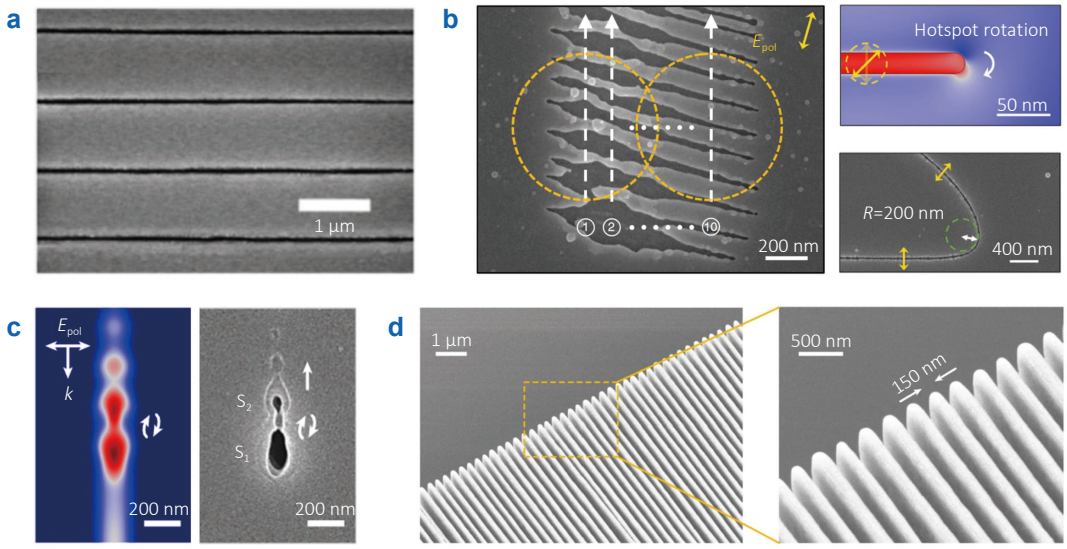

Fig. 6 | (**a**) Nanogroove direct writing with a width less than 40 nm on the surface of ZnO crystal. (**b**) Defect-guided nanostructuring along the electric field enhancement direction. (**c**) Back-scattering interference crawling mechanism based on multiple pulses incubation. (**d**) Silica nanogratings with a period of 300 nm. Figure reproduced from: (a) ref.[81], (b) ref.[25], under a Creative Commons Attribution License; (c, d) ref.[83], Spring Nature.

nanomachining strategies.

Incubation effect of MHz femtosecond laser based on heat accumulation

Due to the short pulse interval of MHz femtosecond laser, apart from the incubation effect resulting from defects accumulation, there is also thermal incubation caused by heat accumulation between adjacent pulses. Unique oxidation patterning and nanostructure synthesis can be achieved through intense thermal oxidation. In addition, the MHz femtosecond laser has shown unique advantages in flexible nanopatterning and 3D patterning. This section introduces the applications based on thermal incubation effect in the above fields.

Oxidation structure patterning

For laser processing operating in ambient air, the laser ablation is often accompanied by intense oxidation. Laser-induced oxidation is often considered as a side effect of laser ablation, for example, it affects the performance of silicon solar cells[84]. However, as the laser repetition rate increases, the heat accumulation between the adjacent pulses can render the laser-induced oxidation dominant. Through parameter optimization, the functional oxidation micro/nano-structures patterning can be achieved. Ma et al. fabricated the convex grid-patterned microstructures on the silicon substrate by high-repetition-rate femtosecond laser irradiation assisted with chemical etching[85]. By controlling laser fluence below the ablation threshold, the silicon oxide patterning can be realized. Due to the difference of reaction rates between silicon oxide and silicon in KOH solution, silicon oxide can be used as an etch stop layer for maskless lithography. As the etching time increases, the structure base shrinks due to the anisotropic etching, thus forming suspended structures[86]. Therefore, the aspect ratio of the structures prepared by wet etching is limited. Since the laser oxidation is accompanied by ablation, there is a distinct laser ablation groove in the middle of the laser formed oxide layer. To overcome these problems, Yin et al. proposed a strategy of seed-guided high-repetition-rate femtosecond laser oxidation combined with deep reactive ion etching to prepare high aspect ratio three-dimensional structures[26]. Defects are firstly generated on the silicon substrate through high fluence laser irradiation, and these defects become the seeds of subsequent laser oxidation. The high absorption regions provided by the seeds enable low fluence laser oxidation under multiple pulses irradiation, which avoids laser ablation and eliminates ablation grooves. Flat oxide layers can be formed by adopting the seed-guided laser oxidation strategy, as depicted in Fig. 7(a). The laser fabricated oxide layers can be used as etching masks. Eventually, high aspect ratio three-dimensional grating structures with ideal beam diffraction characteristics were fabricated by deep reactive ion etching, as shown in Fig. 7(b). This provides an efficient and flexible patterning method for the fabrication of functional three-dimensional silicon structures. Laser oxidation also shows the potential of nanopatterning. Qiao et al. proposed a method to realize titanium oxide nanopatterning on titanium substrate by laser oxidation, and discussed the application potentials of titanium oxide nanostructures in surface coloring and optical encryption[87]. The mechanism behind the oxidation nanostructures formation was analyzed based on the finite difference time domain (FDTD) method. When there is a structure in the laser irradiation area with a size smaller than laser wavelength, the laser intensity is redistributed.

Similar to the defect-guided nanostructuring through laser ablation, the oxidation nanostructuring can also be realized along the direction of laser intensity enhancement. Through this strategy, a "THU" pattern at a characteristic size of 790 nm was realized on the titanium surface, as illustrated in Fig. 7(c).

In addition to achieving oxidized structuring through laser direct writing, researchers have also succeeded in preparing oxidation LIPSS[88]. Due to the distortion of surface electromagnetic wave by ablation debris, the uniformity of LIPSS produced during laser ablation is disturbed[89]. Laser oxidation greatly reduces the surface debris, thus improving the uniformity of LIPSS[90]. Öktem et al. proposed a strategy to regulate oxidation LIPSS through positive and negative feedback[91]. The positive feedback stems from the influence of the substrate surface structures on the laser intensity distribution. Oxidized nanostructures form in the regions with an enhanced laser intensity, and these structures continue to affect the intensity distribution of subsequent laser pulses, as shown in Fig. 7(d). The growth mechanism contains a negative feedback loop. As titanium dioxide grows on the titanium surface, the penetration of oxygen through the oxide layer decreases exponentially, slowing down and eventually halting the oxidation LIPSS growth. Large-area nanostructuring of titanium dioxide can be realized by using feedback adjustment strategy. Using high-repetition-rate femtosecond laser to prepare oxidation structures in ambient air has attracted extensive attention. In the future, exploring the interaction processes between materials and gases under different atmospheres will offer new perspectives for the laser precision engineering.

Nanostructure synthesis

Functionalized nanomaterials have attracted extensive research interest in the fields of biosensing and energy harvesting etc., owing to their unique properties that bulk materials lack[92,93]. Femtosecond laser ablation in ambient air is a complex explosive process, accompanied by substrate materials removal and nanoparticles synthesis. In the process of high-repetition-rate femtosecond laser ablation, a large number of oxide nanoparticles are generated on both sides of the scanning path[94]. Thakur et al. reported a strategy of synthesizing titanium oxide nanomaterials on the substrate surface to broaden and enhance the surface absorption[95]. Self-assembled multiphase titanium oxide nanoparticles were formed by the high-repetition-rate femtosecond laser incubation, as shown in Fig. 8(a). The

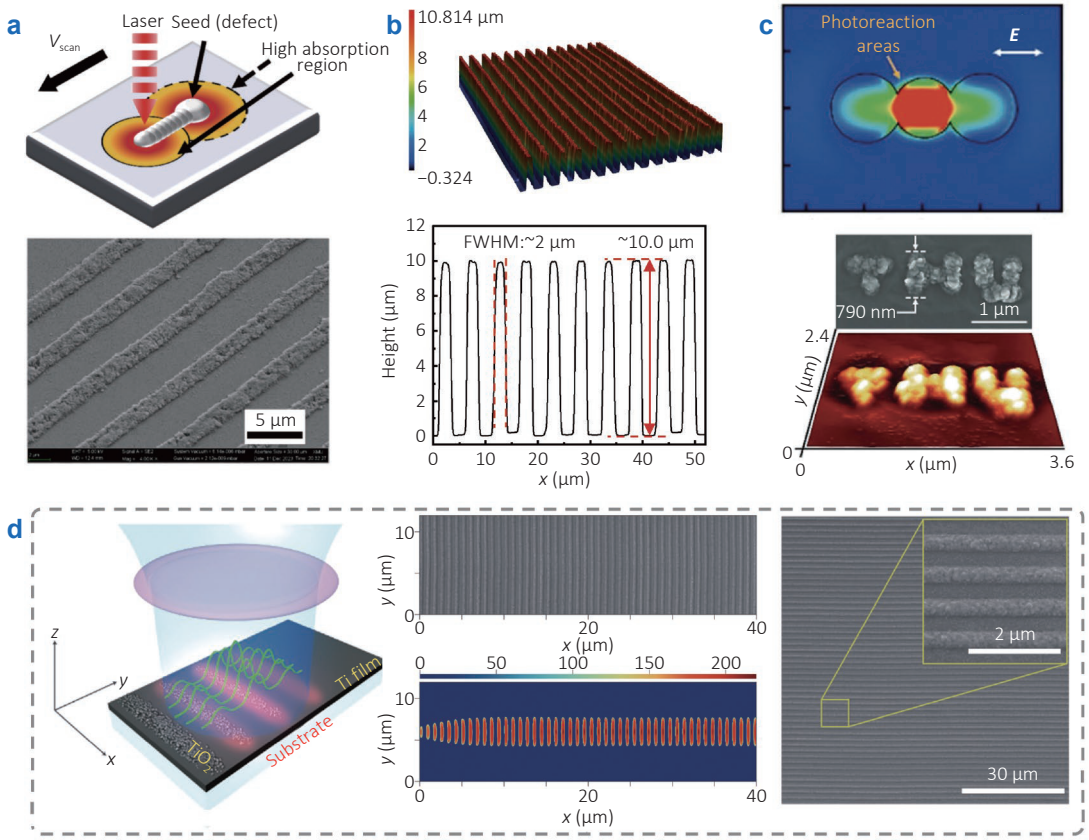

Fig. 7 | (**a**) Flat oxide layers formed by seed-guided laser oxidation. (**b**) High aspect ratio three-dimensional grating structures fabricated by deep reactive ion etching. (**c**) Formation mechanism of oxidized nanostructures and the fabricated TiO_2 nanostructures. (**d**) Large-area nanostructuring of titanium dioxide realized by feedback adjustment strategy. Figure reproduced from: (a, b) ref.[26], Elsevier; (c) ref.[87], John Wiley and Sons; (d) ref.[91], Spring Nature.

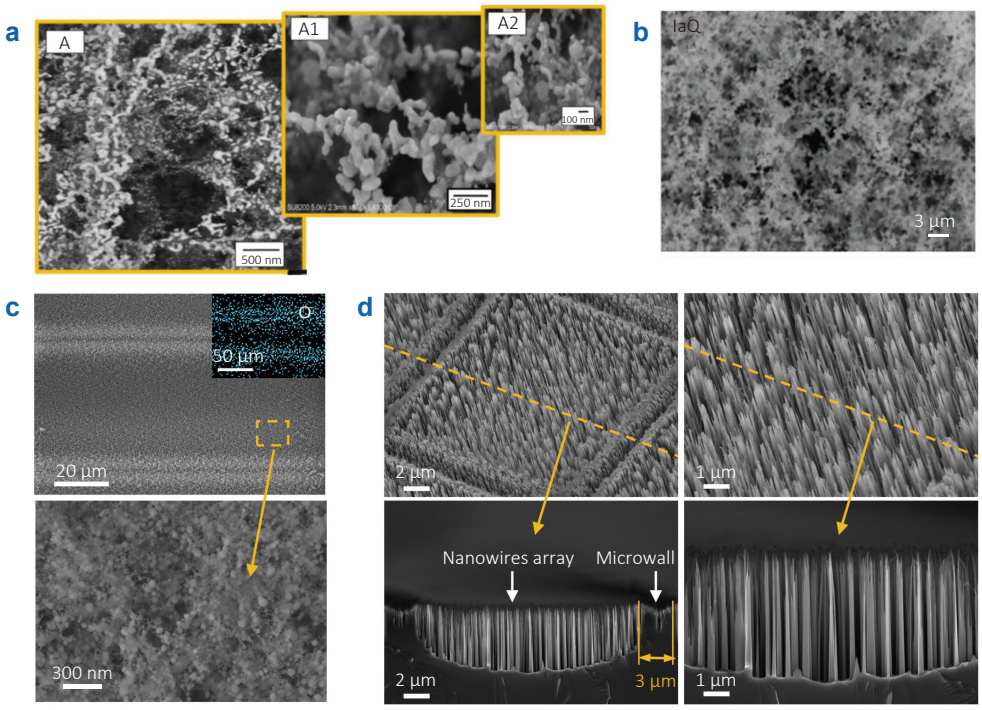

Fig. 8 | (**a**) Self-assembled multiphase titanium oxide nanoparticles formed by femtosecond laser incubation. (**b**) Titanium oxide nanoparticle probes with atomic-level defects synthesized by femtosecond laser ablation. (**c**) Micro/nanocross-scale silicon oxide mask manufactured by femtosecond laser in a single step. (**d**) Armored silicon nanowires array for SERS detection. Figure reproduced from: (a) ref.[95], (b) ref.[96], Elsevier; (c, d) ref.[27], American Chemical Society.

synthesized nanostructures promote the overall enhancement of the absorption of the solar energy in the visible and near-infrared regions ranging from 300 nm to 1000 nm. Dharmalingam et al. proposed a method to synthesize titanium oxide nanoparticle probes with atomic-level defects via laser irradiation, which can be used for the trace detection of cancer biomolecules[96]. Nanoparticle probes with oxygen vacancy defects were synthesized by high-repetition-rate femtosecond laser ablation, as illustrated in Fig. 8(b). Through the cooperative control of laser fluence and pulse repetition rate (2, 8 and 25 MHz), the defects density can be adjusted. High-density defects in the nanoparticle probes significantly improve the detection sensitivity of molecules.

Nanostructures synthesized by laser can also be transferred to the substrate. Yin et al. manufactured a micro/nanocross-scale silicon oxide mask in a single step by using the oxide layer and oxide nanoparticles generated during laser processing[27]. The oxide mask mainly consists of two parts: one is the dense oxide layer at the laser scanning path, and the other is the porous nanoparticles layer between the scanning paths, as shown in Fig. 8(c). Combined with the optimized deep reactive ion etching, the armored silicon nanowires array for robust surface-enhanced Raman scattering (SERS) detection was prepared, as illustrated in Fig. 8(d). The armored nanostructures substrate exhibits a high contact angle (158°) and shows the ability to enrich analytes. The detection limit for Rhodamine 6G is 10^{-13} M, and the enhancement factor is 4.35×10^{9}. The armored nanostructures, in which the nanostructures are embedded inside interconnected microstructures, significantly improve the mechanical properties of the nanostructures. Through various mechanical tests (water impact, pressurization, and tape peeling), the substrate can still exhibit stable Raman signal enhancement. High-repetition-rate femtosecond laser has shown the potentials to synthesize oxidation nanostructures, and its advantages can also be explored in laser nitriding, laser carbonization, and other fields in the future[97,98].

Flexible nanopatterning

Achieving nanopatterning in far field and ambient air through optical means is of great significance for the laser precision engineering. He et al. precisely controlled the laser fluence to balance the relationship between surface plasmon interference and surface thermal stress, achieving patterning from four-line to a single-line nanogrooves[99], as shown in Fig. 9(a). Due to the laser Gaussian intensity distribution, the temperature of SU-8 (coated on quartz) in the irradiated central area rises significantly. Under the action of surface thermal stress, nanogroove at a feature size of only 40 nm are realized on the SU-8 surface. In addition, the hybrid laser method has shown the potentials for nanoprocessing on various materials[100,101]. Lin et al. proposed an innovative strategy to achieve features at a size

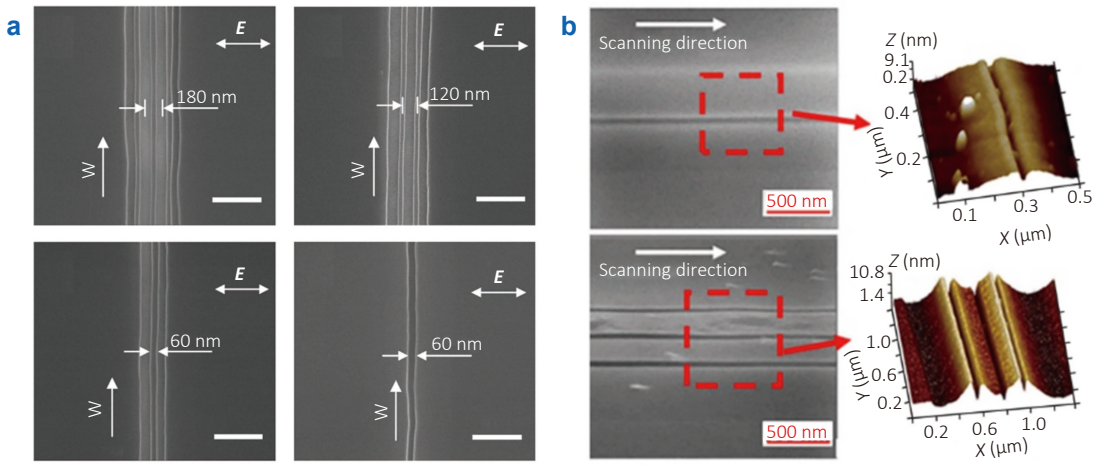

Fig. 9 | (**a**) Four-line to single-line nanogrooves realized on SU-8 surface by surface thermal stress. (**b**) Single-line and triple-line nanogrooves achieved on silicon surface through the thermal incubation of orthogonally polarized double laser beams. Figure reproduced with permission from: (a) ref.[99], under a Creative Commons Attribution License; (b) ref.[23], American Chemical Society.

of 12 nm on the silicon surface using orthogonally polarized double high-repetition-rate femtosecond laser beams[23]. By controlling laser fluence and the gap between the double laser beams, the preparation of nanogrooves from single-line to multi-line can be realized, as illustrated in Fig. 9(b). The incubation effect based on multiple femtosecond laser irradiations at a high repetition rate (76 MHz) is considered to be the main reason for the formation of approximately 10 nm nanostructures. Through the multiple pulses thermal incubation, the heat accumulation can be controlled near the materials melting threshold. By utilizing the surface tension of the liquid from the edge to the center, the melting area is reconstructed, thus realizing the surface nanostructuring.

An important factor limiting the further reduction of laser processing size stems from the optical diffraction limit. The focused laser spot is limited by laser wavelength and the numerical aperture of objective lens. Researchers have found that when light passes through dielectric microspheres, sub-wavelength photonic nanojets (PNJ) can be generated[102,103]. Microspheres have been widely used in optical nanoimaging and have improved the far field optical imaging resolution from 200 nm to sub-50 nm[104,105]. Microsphere assisting laser processing is also a promising technique for far field nanostructuring[106]. Lin et al. achieved sub-50 nm surface nanostructuring on Sb_2S_3 films via microsphere-assisted high-repetition-rate femtosecond laser irradiation in far field and ambient air[28], as illustrated in Fig. 10(a). The formation of these nanostructures is attributed to the combined effects of the sub-wavelength focusing of microsphere, the non-linear absorption of femtosecond laser, and the incubation effect based on high-repetition-rate femtosecond laser irradiation. By precisely controlling the scanning speed and laser fluence, the minimum feature size can be reduced to approximately 30 nm. This strategy allows writing triple nano-lines at a period of 150 nm, indicating that highly integrated nanostructuring can be achieved, as shown in Fig. 10(b). Furthermore, combining smaller microspheres with higher refractive index can potentially improve the machining accuracy down to 10 nm. Liu et al. proposed a switchable color printing method using Sb_2S_3-based step-pixelated Fabry-Pérot (FP) cavities realized by laser patterning[107]. By accurately controlling the Sb_2S_3 thickness in the FP cavity via laser, various colors can be realized. Eventually, a "Bing Dwen Dwen" color display was fabricated based on the database of the relationship between laser fluence and Sb_2S_3 thickness, as depicted in Fig. 10(c). As the switching between the crystalline and amorphous Sb_2S_3 can cause a significant change in the refractive index within the visible light range, the color variation of the display can be realized. Combined with microsphere femtosecond laser irradiation, the minimum patterning size can be reduced to approximately 48 nm, which provides guidance to realize nano-resolution color display, as shown in Fig. 10(d).

3D micro/nano-printing

Realizing 3D micro/nano-printing by femtosecond laser has been applied to the preparation of functional devices, such as optical lenses and optical sensors[108,109]. The two-photon absorption based on the non-linear effect of femtosecond laser further improves the printing resolution. In the nonlinear interaction between femtosecond laser and materials, the probability of multiphoton absorption is directly proportional to laser repetition rate[110,111], the high repetition rate laser can realize sub-diffraction limit printing more efficiently and controllably. Du et al. proposed a method of mixing nanomaterials with photoresist, which realized the customized material properties of the printed structure[29]. By mixing silica nanoparticles, the mechanical properties of printed structures are improved, and it is

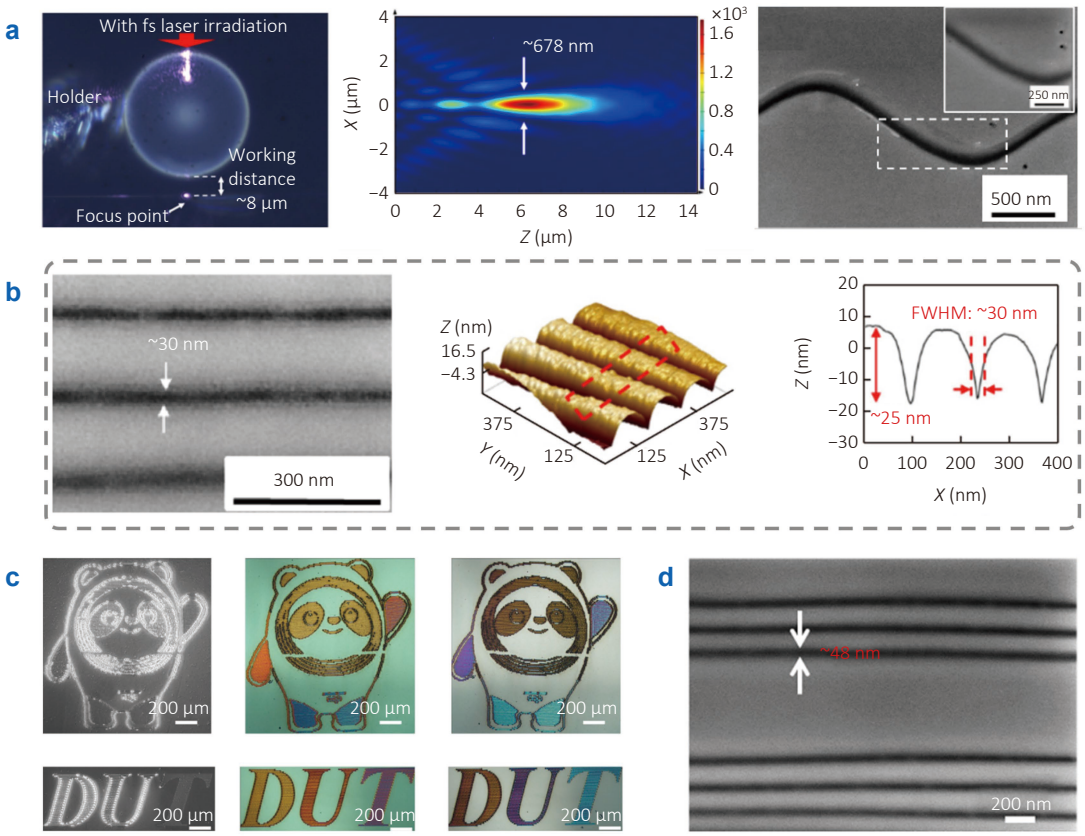

Fig. 10 | (**a**) Sub-50 nm surface nanostructuring on Sb_2S_3 films achieved by microsphere-assisted high-repetition-rate femtosecond laser irradiation. (**b**) Triple nano-lines at a period of 150 nm realized on the Sb_2S_3 film surface. (**c**) A "Bing Dwen Dwen" color display with color variation function. (**d**) Super-resolution nano-lines formed by microsphere femtosecond laser irradiation. Figure reproduced with permission from (a, b) ref.[28], (c, d) ref.[107], under a Creative Commons Attribution License.

possible to prepare highly customized multilayer micro/nano-structures. The mixed photoresist can be regarded as micro-concrete, and the 3D Eiffel Tower was prepared by multilayer printing, as illustrated in Fig. 11(a). Gold nanoparticles can also be mixed into photoresist, thus realizing the printed structure with adjustable light trapping ability. This indicates that femtosecond laser 3D printing has the ability to fabricate various functional structures. In the process of evolution, nature always produces various structures with extraordinary functions, providing references for various unique applications in real life. Calin et al. reported a laser 3D printing method for microlens arrays inspired by the eyes of the nocturnal moth *Grapholita Funebrana*[112]. The surface of the bionic moth-eye microlens is covered with nanopillars between 200 nm and 400 nm in height and less than 100 nm in diameter, as shown in Fig. 11(b). Compared with microlens without nanopillars, the infrared light transmittance of the bionic moth-eye microlens in the range of 1000 nm to 1700 nm is increased by 17.55%, which can be applied to infrared optical detection. Zhang et al. proposed a strategy to manufacture intelligent variable 3D micro-actuators based on femtosecond laser printing optical polymers[113]. By optimizing the femtosecond laser processing parameters, the 3D distribution and size of voxels can be accurately controlled. Through the precise programming of the laser scanning path, a microclaw array with 8 intelligent fingers was fabricated[113], as shown in Fig. 11(c). The microclaws can achieve the function of grasping and releasing, similar to the mollusk muscles. Due to the flexibility of femtosecond laser manufacturing, the microclaws can be integrated to quartz microfibers, demonstrating application potentials in on-chip systems. Moreover, natural musculoskeletal systems are an advanced model to realize robust and flexible microrobots. Ma et al. manufactured 3D microrobots through the artificial musculoskeletal systems printed by femtosecond laser[114]. They used SU-8 as the skeleton and pH-responsive protein (bovine serum albumin, BSA) as the muscle. Through a continuous on-chip two-photon polymerization strategy, the orderly construction of two photosensitive materials can be realized. Figure 11(d) illustrates a spider microrobot realized by the artificial musculoskeletal system. Spider robot consists of SU-8 body and eight SU-8 skeletal legs. There is a vacancy at the junction of each leg in order to integrate the muscles formed by BSA. When the pH value of the surrounding medium is changed, the BSA muscle responds, thereby enabling the actuation of the micro spider. In addition to SU-8 and BSA, this general

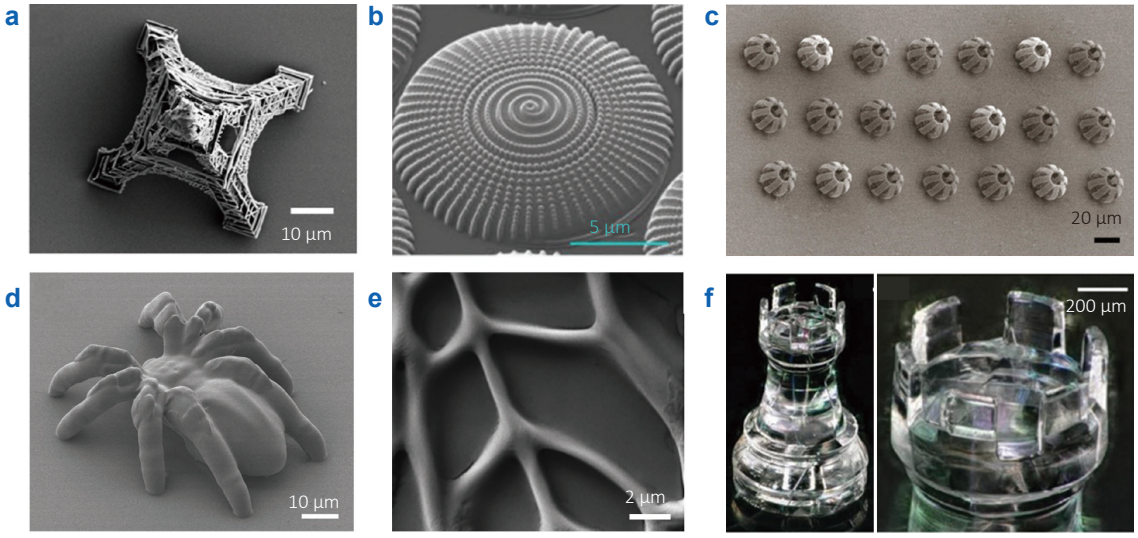

Fig. 11 | (**a**) 3D Eiffel Tower prepared by multilayer printing. (**b**) Bionic moth-eye microlens decorated with nanopillars. (**c**) Microclaw array with 8 intelligent fingers prepared based on optical polymers. (**d**) A spider microrobot realized by the artificial musculoskeletal system. (**e**) Micro-maple leaf structure with clear veins fabricated by poly(ionic liquid)s. (**f**) 3D triangular truss structures of fused silica glass. Figure reproduced with permission from: (a) ref.[29], Institute of Electrical and Electronics Engineers; (b) ref.[112], under a Creative Commons Attribution License; (c) ref.[113], American Chemical Society; (d) ref.[114], under a Creative Commons Attribution License; (e) ref.[115], Elsevier; (f) ref.[116], John Wiley and Sons.

strategy also allows for the programmable integration of multiform materials into complex 3D microstructures, holding promise for the fabrication of other functional structures. Tudor et al. prepared a soft stimulus-responsive 3D structure with submicron resolution via the laser printing of poly(ionic liquid)s (PILs)[115]. Figure 11(e) shows the micro-maple leaf structure with clear veins fabricated based on the above strategy. By absorbing and releasing solvents, the whole leaf structure can be greatly changed, and the structural integrity can be well maintained during the actuation cycle.

In addition to femtosecond laser 3D printing based on polymer materials, researchers are also exploring printing strategies for inorganic materials, such as metals, glasses, and ceramics[117,118]. By preparing composite ink mixed with inorganic materials and two-photon polymerizable materials, three-dimensional molding of inorganic materials can be realized[116]. By precisely controlling the reaction chamber temperature, the polymer is first removed through a pyrolysis process, and then the structure is shrunk and the voids left after the polymer pyrolysis are eliminated through a sintering process, finally resulting in an inorganic 3D structure, as depicted in Fig. 11(f). Deformation compensation and porosity control during the sintering process are challenging issues[119]. Wang et al. proposed a printing strategy for complex 3D metal structures without polymers, which is based on femtosecond laser-induced two-photon decomposition, optical force trapping, and ultrafast sintering of nanocrystals[120]. The energy density at the laser focal point enables two-photon absorption, causing the decomposition of metal carbonyls and generating free Mo, Co, and W atoms. These free atoms rapidly assemble under van der Waals forces to form nanoclusters. Under the action of high-repetition-rate femtosecond laser, the nanoclusters undergo rapid sintering and cooling, ultimately producing a dense and smooth nanostructure. 3D printing has emerged as one of the most powerful strategies in femtosecond laser precision engineering, and how to further improve processing efficiency and increase throughput should be considered as well in the future research.

Incubation effect of GHz femtosecond laser based on plasma interaction

With the development of laser technology, the recent ability to generate femtosecond laser pulses at GHz repetition rate has opened up new possibilities for laser precision engineering[121,122]. Increasing the laser repetition rate can enhance the output of laser processing to meet the needs of industrial applications[123]. Meanwhile, the extremely low pulse interval makes the plasmas interaction between pulses become possible, which realizes new machining strategies based on the incubation mechanism. This section summarizes the various applications of the incubation effect for GHz femtosecond lasers based on the plasmas interaction.

High efficiency materials removal

When the material is ablated, the thermal energy in the ablated mass is also removed, thus reducing the average temperature of the remaining materials. Kerse et al. proposed a novel ablation-cooled materials removal strategy based on GHz femtosecond laser irradiation[30]. When the laser repetition rate is low, the material in the processing area is cooled by thermal diffusion before the

subsequent pulse irradiation, which leads to the loss of deposited laser energy and hinders the improvement of laser processing efficiency. When the time interval between adjacent pulses is short enough, such as picosecond, there is significant heat accumulation between adjacent pulses. Subsequent pulses can ablate heated materials at a lower laser fluence, so the machining efficiency is significantly improved. Since there is no significant thermal diffusion during the processing, the HAZ is smaller. The hard tissue ablation experiment of human dentin shows that the ablation rate of the ablation-cooled strategy is four times higher than that of the traditional regime, and there is no obvious thermal damage on the materials surface, as indicated in Fig. 12(a). This strategy can also be applied to other materials, such as Si, Cu, PZT, and PMMA. The high-quality cutting achieved on copper foil at a thickness of 20 μm is shown in Fig. 12(b). Bonamis et al. explored the efficiency and quality of the GHz femtosecond laser ablation of copper, aluminum and stainless steel[124]. The comparison of ablation results between GHz femtosecond laser and nanosecond laser on copper substrates is shown in Fig. 12(c). The GHz burst pulse train contains 100 pulses at a 0.88 GHz intraburst repetition rate. The total duration of a pulse train is 114 ns and total laser fluence is 9.7 J/cm^2. The pulse duration of nanosecond laser is 100 ns and the laser fluence is 4.7 J/cm^2. The results show that the ablation efficiency of GHz burst femtosecond laser is equivalent to nanosecond laser while the machining quality is much higher. The ablation threshold (0.03 J/cm^2) in burst mode is 15 times lower than that in single pulse mode (0.4 J/cm^2). There is a new incubation ablation mechanism for this low laser fluence ablation. Before the laser ablation, the material first goes

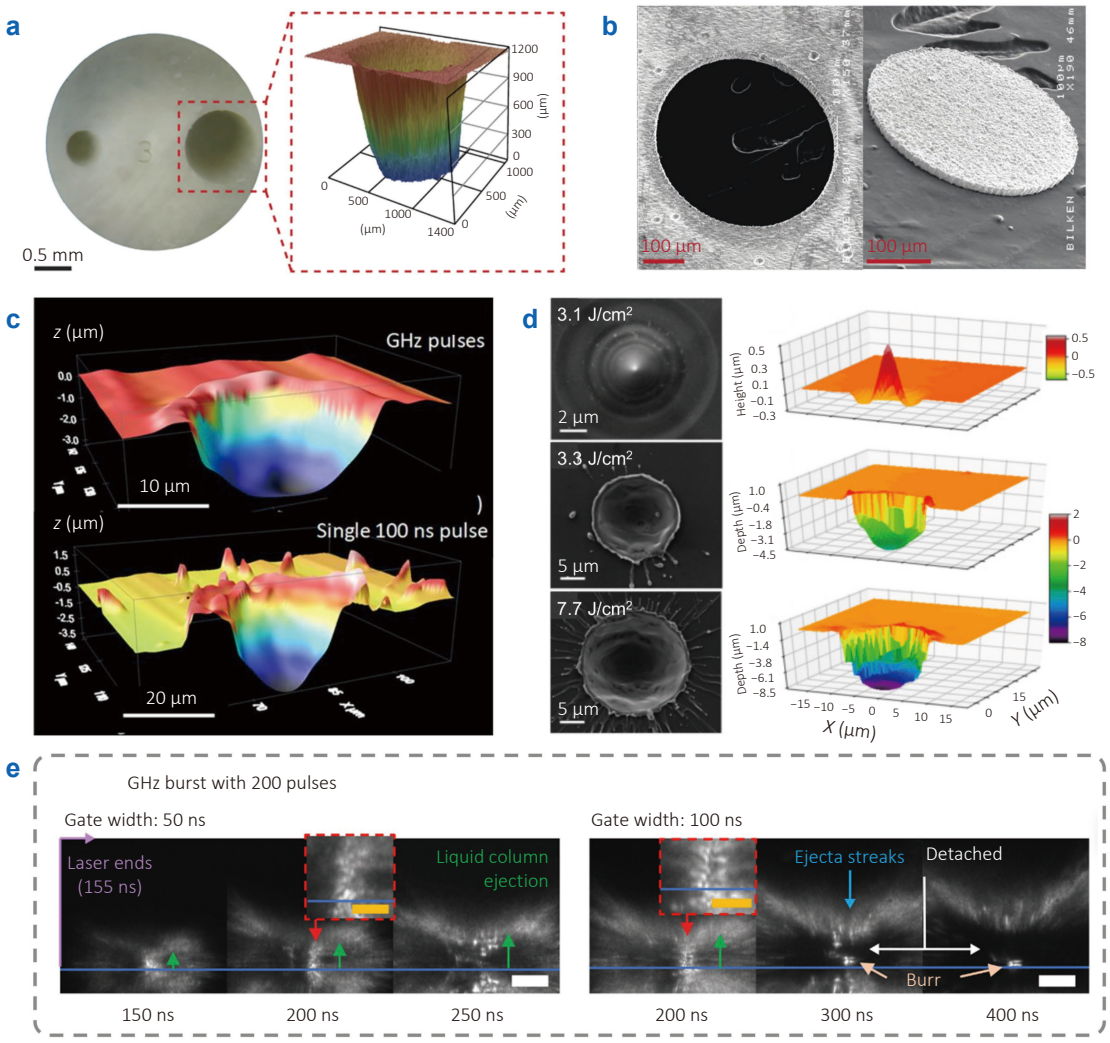

Fig. 12 | (**a**) Tissue removal of human dentin in ablation-cooled regime. (**b**) High-quality cutting on copper foil based on ablation-cooled strategy. (**c**) Comparison of ablation results between GHz femtosecond laser and nanosecond laser on copper substrate. (**d**) Two modification types of burst mode femtosecond laser found on the silicon surface: bumps formation at low laser fluence and ablation craters formation at high laser fluence. (**e**) Dynamics of Cu ablation by GHz femtosecond laser. Figure reproduced from: (a, b) ref.[30], Spring Nature; (c) ref.[124], American Institute of Physics; (d) ref.[125], Optical Society of America; (e) ref.[126], American Association for the Advancement of Science.

through the heating process, which is guided by pulses far below the materials ablation threshold. With the increase of pulse number, the materials ablation threshold gradually decreases. When the materials temperature reaches the critical value, the subsequent pulse low fluence can trigger the materials ablation. The pulse interval is short enough to cause almost no heat dissipation between pulses, so that high efficiency ablation can be realized. Mishchik et al. achieved a high efficiency ablation of 25 $mm^3 \cdot min^{-1} \cdot W^{-1}$ on silicon with a burst mode femtosecond laser containing 200 pulses at 0.88 GHz, and discussed the contribution of multiple pulses incubation to materials ablation in burst mode[125]. Two modification types of burst mode femtosecond laser irradiation were found on the silicon surface: bumps formation at a low laser fluence and ablation craters formation at a high laser fluence, as indicated in Fig. 12(d). With the increase of pulse number in the pulse train, the formation thresholds of both structures decrease, which further proves the contribution of incubation effect in GHz burst mode femtosecond laser processing.

The reduction of the thermal effect and the improvement of the ablation efficiency in GHz femtosecond laser ablation have shown unique potentials in industrial applications[127]. However, there is still controversy about the specific ablation mechanism, and it is necessary to directly detect the complex process of light-matters interaction through in-situ characterization. Park et al. realized the real-time detection of GHz femtosecond laser ablation dynamics through multimodal collaborative diagnosis of scattering imaging, emission imaging, and optical emission spectroscopy[126]. Through real-time detection, it is found that the recoil pressure exerted by the subsequent pulse of GHz femtosecond laser leads to the rapid removal of molten materials, as shown in Fig. 12(e). This introduces a novel insight into the complex mechanism of femtosecond laser ablation in GHz burst mode.

In addition to materials such as metal and silicon, GHz femtosecond laser also shows unique advantages in dielectric processing. Lopez et al. fabricated high-quality deep holes machining on glass by GHz femtosecond laser irradiation, and revealed the percussion drilling dynamics by pump-probe shadowgraphy and thermal imaging[128]. The temperature change around the drilling hole was recorded by a thermal imager, and an obvious cycle of heating and ablation was observed, as shown in Fig. 13(a). There are 26 "materials ejections"[128] during the drilling process, which showed that the percussion drilling is carried out in a progressive way in the burst mode. Similar to the low fluence ablation of GHz femtosecond laser, the pre-heating of the initial pulse reduces the drilling threshold. By optimizing the laser processing parameters, the deep hole at an aspect ratio as high as 20 can be fabricated. Balage et al. made a systematic comparison of single pulse, MHz- and GHz-burst regimes ultrafast laser drilling by pump-probe imaging[129]. The ablation plume in the state of GHz explosion plays a vital role in the drilling process. The energy distribution of the pulse sequence of the GHz burst mode femtosecond laser also has a great influence on the machining results. Balage et al. explored the influence of the burst shape of GHz femtosecond laser on drilling[130]. By adjusting the energy distribution of each pulse in the pulse train, the burst shape of the pulse train can be changed. The decreasing burst shape, increasing burst shape and flat burst shape are realized as indicated in Fig. 13(b). When the decreasing burst shape is adopted, the drilling rate is improved, but the maximum depth of the hole is reduced, and some cracks appear around the inner wall of the hole. In this configuration, the first pulse carries more energy and the initial heat accumulation is obvious. It shows a higher drilling speed at first. With the interaction of subsequent pulses, the enhanced plasma leads to the intensification of shielding effect, which affects the maximum drilling depth. For the pulse trains with increasing or flat burst shapes, the materials can be heated more evenly during the punching, and the heat accumulation can be better controlled. In this way, the holes not only have a greater depth, but also have a smoother inner wall, showing excellent processing quality.

Some researches found that the enhancement in machining efficiency for scribing and milling is less significant than that for drilling[131,132]. Schwarz et al. utilized GHz burst femtosecond laser to investigate the influence of different burst pulse numbers on the milling efficiency of fused silica[133]. As the burst pulse number increases, the ablation efficiency improves significantly. For the burst pulse number of 10, the maximum ablation rate (3.05 $mm^3 \cdot min^{-1} \cdot W^{-1}$) is obtained, which is 7.4 times as high as that of the non-burst mode (0.41 $mm^3 \cdot min^{-1} \cdot W^{-1}$). Additionally, the roughness of the milling surface also increases with pulse number, as shown in Fig. 13(c). Taking into account the surface machining quality and machining efficiency, the ablation rate can be increased by 3.5 times with a better surface quality at the burst pulse number of 5. The processing efficiency improvement via GHz femtosecond laser irradiation also depends on the intrinsic properties of materials, such as bandgap[132], which requires the different optimal pulse train configurations to realize desirable nanostructuring on different materials[134,135].

Although direct laser ablation has been widely used in the precision engineering of various materials, it causes damage and cracks on transparent materials due to their weak light absorption[136]. To realize high-quality transparent material processing, laser-induced plasma-assisted ablation (LIPAA) has become an effective strategy[137,138]. Different from the traditional laser processing strategies, LIPAA enhances the laser absorption of transparent materials through the plasma generated by the interaction between incident laser and target on the backside of the transparent material[139,140]. The intensity of laser-generated plasma significantly affects the ablation efficiency. Researchers have proposed several methods to enhance the

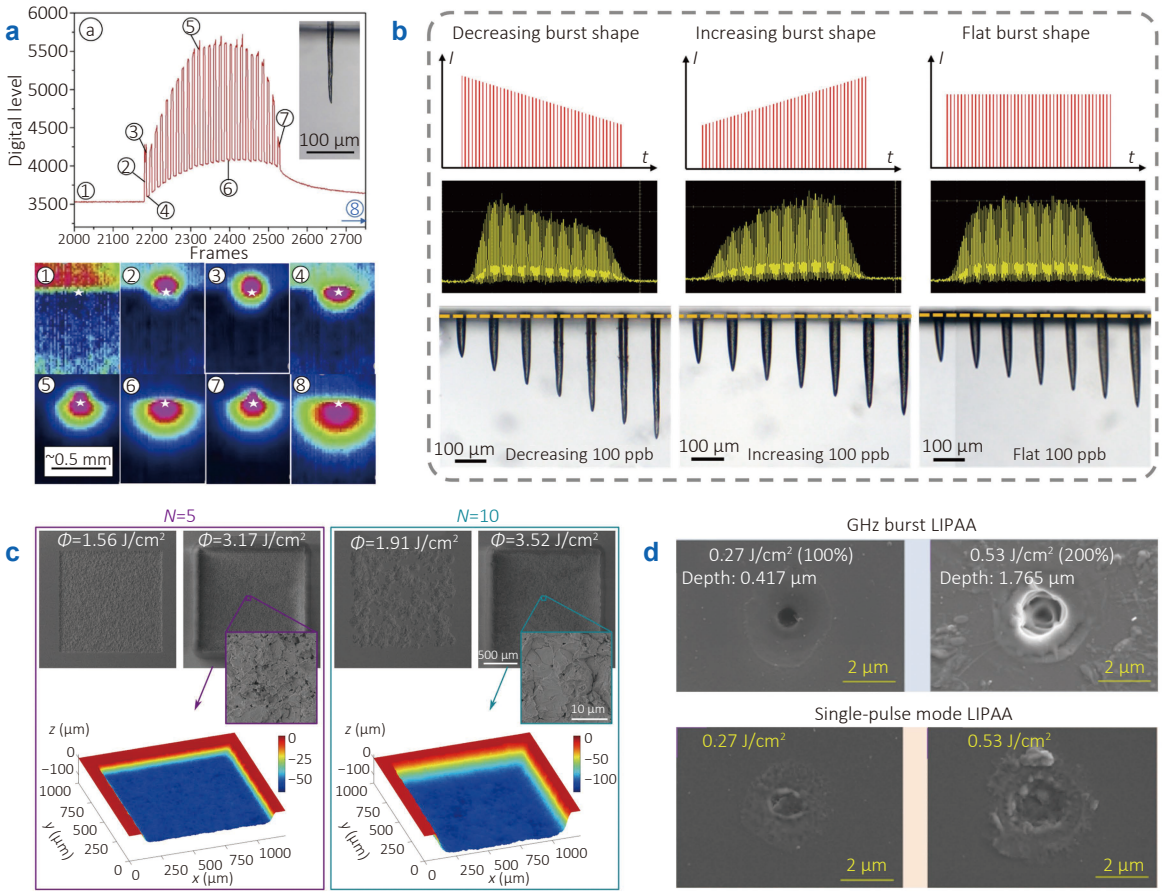

Fig. 13 | (**a**) Temperature change around the drilling hole recorded by the thermal imager. (**b**) Influence of burst shape of GHz femtosecond laser on drilling effect. (**c**) Variation of milling surface morphology with the increase of pulse number. (**d**) Ablation craters produced by GHz burst LIPAA and single-pulse mode LIPAA on sapphire substrate. Figure reproduced with permission from: (a) ref.[128], (b) ref.[130], (d) ref.[51], under a Creative Commons Attribution License; (c) ref.[133], Optical Societyof America.

plasma interaction with the glass substrates and improve the processing efficiency[141]. The interaction between plasmas induced by double-beam laser irradiation promotes plasma dynamic, forming a larger and stronger plasma[142]. Obata et al. realized the high-resolution and efficient ablation of sapphire by applying GHz burst mode femtosecond laser[51]. Due to the pulse interval being on the picosecond order, the subsequent pulses can directly interact with the plasma generated by the previous pulses. The high efficiency ablation can be achieved for the burst mode LIPAA. The ablation craters produced by GHz burst LIPAA and single-pulse mode LIPAA on sapphire substrate are shown in Fig. 13(d). The surface obtained by single-pulse mode LIPAA is much rougher. Under the GHz burst LIPAA, the enhanced plasma causes more effective absorption on the sapphire surface, resulting in a higher absorption and the subsequent better ablation quality. The ablation depth of the GHz burst LIPAA is 4–5 times deeper than that of the single pulse mode LIPAA. Meanwhile, the multiple pulses incubation of the burst mode LIPAA achieves high-quality processing of sapphire. In future, this strategy can be extended to other transparent materials to explore its further potential application.

Burst mode surface texturing

In addition to achieving high-efficiency and high-quality materials removal, some researchers have explored the laser texturing strategy via GHz burst mode to gain new insights for surface engineering[143,144]. Gaidys et al. realized high-speed laser coloring to make blue, purple, and orange colors on stainless steel surfaces by GHz femtosecond laser irradiation[145]. Ultra-high laser pulse repetition rate allows a higher scanning speed in the laser coloring at a speed of 42.5 mm²/s. Laser irradiation in burst mode is beneficial to heat accumulation and can accelerate the oxidation, thus forming an oxide layer on the stainless steel surfaces. Due to thin film interference between oxide layers, the stainless steel surface can show different colors[146]. Kawabata et al. obtained two-dimensional (2D) LIPSS on silicon surface by GHz femtosecond laser irradiation[31]. LIPSS formed by a linearly polarized single pulse laser irradiation is usually perpendicular to the polarization direction. However, the GHz femtosecond laser with specific burst pulse number can produce a unique 2D-LIPSS, as shown in Fig. 14(a). The mechanism behind is attributed to the synergistic effect of electromagnetism and fluid dynamics. There is an obvious

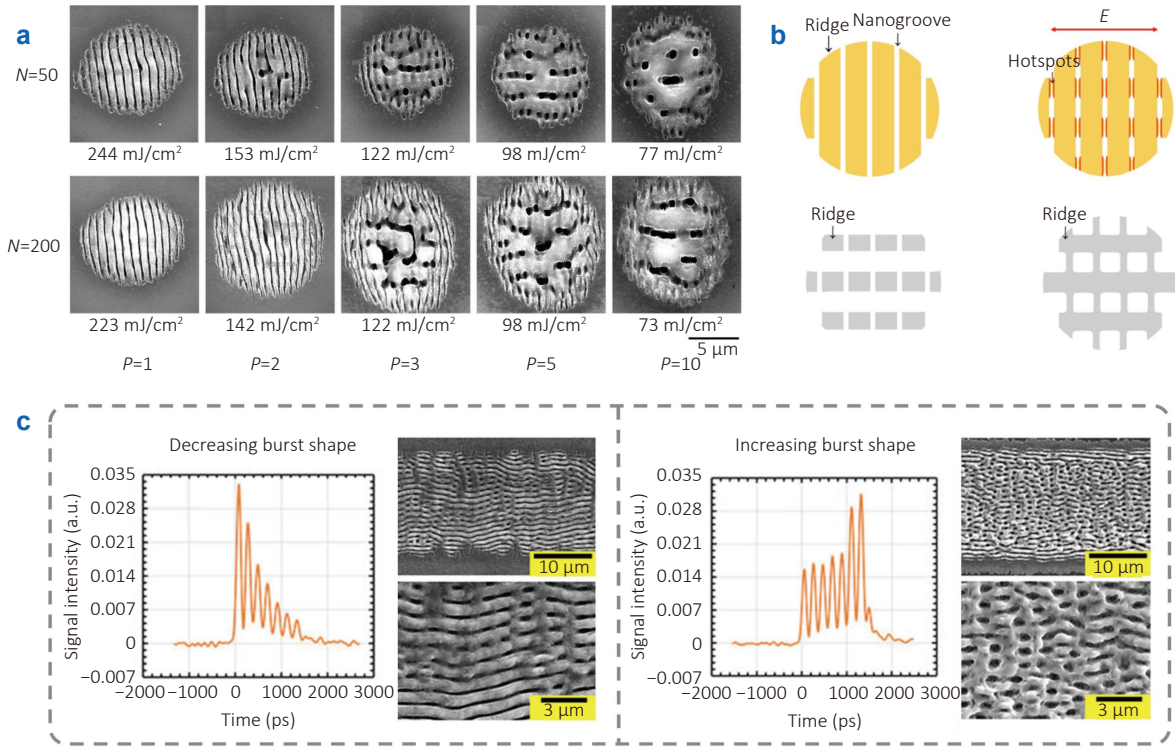

Fig. 14 | (**a**) 2D-LIPSS fabricated on silicon surface by GHz femtosecond laser irradiation. (**b**) Localized surface plasmon resonance in 1D-LIPSS. (**c**) Influence of burst shape on 2D LIPSS morphology. Figure reproduced with permission from: (a, b) ref.[31], (c) ref.[147], under a Creative Commons Attribution License.

recast layer formed by melting and re-solidification in the central area of the 2D-LIPSS, which comes from the heat accumulation under GHz burst mode. The distribution of the recast layer exhibits a certain regularity, which originates from the hot-spots generated in specific regions within the 1D-LIPSS due to the local surface plasmon resonance (LSPR). The 1D-LIPSS is first fabricated by the first few pulses of the GHz pulse train. Due to the LSPR, the subsequent pulses generate hot-spots with enhanced electric fields between the structures, which alters the distribution of laser energy. The laser energy in the enhanced regions exceeds the materials melting threshold, leading to the localized melting, and finally a 2D-LIPSS is formed, as shown in Fig. 14(b). Kawabata et al. further proved that the 2D-LIPSS can also be formed on titanium surface by GHz femtosecond laser irradiation when the burst pulse number exceeds 5[147]. By controlling the burst shape, the formation mechanism of the 2D-LIPSS was studied in detail. Three types of decreasing burst shapes (energy distribution with a negative slope) and increasing burst shape (energy distribution with a positive slope) were applied to regulate structure morphology. Similar to the situation on the silicon surface, the electric field enhancement at the hot-spots is an important factor determining the final morphology of 2D-LIPSS. The latter several pulses in the pulse train affect the energy distribution of the hot-spots. Therefore, by changing the energy distribution of the subsequent pulses, the morphology of the 2D-LIPSS can be regulated. If the energy of the subsequent pulses is too weak to enhance the electric field, the 2D-LIPSS cannot be formed, as shown in Fig. 14(c). However, if the energy of the subsequent pulses in the pulse train is too high, the electric field enhancement is too strong, the materials melt significantly, and the regularity of the final structure deteriorates. Controlling the burst shape provides a new perspective to regulate the GHz burst mode surface texturing, and it holds the promise of achieving more complex structures with unique surface functions. In summary, the GHz burst femtosecond laser not only enables unique energy injection during the ablation, but also causes a series of nonlinear phenomena, which opens up a new way for micro/nano-manufacturing.

Challenges, outlooks, and conclusions

Femtosecond laser micro/nano-manufacturing based on multiple pulses incubation has been widely developed and studied in various precision engineering fields. At the forefront of technological development and technology from laboratory to industrial application transformation, there are still several challenges needed to be overcome. The first challenge is how to realize the in-situ observation of the interaction between high-repetition-rate laser and materials. Although researchers have put forward some models of various incubation mechanisms, the dynamic evolution of incubation effect is still not fully understood due to the lack of in-situ characterization method to capture such transient processes. For the defect incubation at kHz, since the

resolution of traditional optical microscope is ~200 nm, which cannot identify the initial nano-defects and the scanning electron microscope lacks the ability of real-time imaging. It is the research direction to solve this problem for real-time nano-imaging beyond the diffraction limit by engineered microspheres optical nano-imagining. For thermal incubation at MHz, the interval between adjacent pulses is tens of nanoseconds. A thermal imaging technology with sub-microsecond frame rate is needed to track the heat accumulation on the materials surface. For the GHz femtosecond laser processing system, besides the thermal incubation, the interaction between adjacent pulsed laser ablation induced plasmas also needs to be investigated in detail. It is necessary to develop a multi-modal real-time monitoring system based on pump-probe measurements, ultrafast imaging, and ultrafast spectroscopy to provide direct insight into the GHz ablation dynamics. The second challenge is the suppression of thermal effect in the high-repetition-rate laser processing. Although the MHz femtosecond laser can realize nano-fabrication through the precise control of thermal stress, excessive heat accumulation under multiple pulses incubation is a long-term challenge in precision manufacturing. Residual heat leads to unexpected materials modification (for example, localized heating exceeding 1000 K in MHz processing will lead to silicon amorphization, coarsening of metal grains, and thermal cracking of ceramics etc.), which affects machining accuracy and surface quality. By adopting pulse energy and spatial beam shaping strategies, accurate thermal control can be realized. For different laser-materials processing systems, laser repetition rate, wavelength and pulse energy distribution should be well matched with the materials characteristics. The photothermal effect and photochemical reaction induced by the femtosecond laser irradiation are expected to further reduce the HAZ. The third challenge is on laser nano-fabrication in GHz burst mode. Although GHz burst femtosecond laser has shown unique advantages of efficient materials removal and surface texturing, there are no relevant reports of GHz laser surface engineering in nano-fabrication (e.g., <100 nm). Sub-picosecond pulse time interval leads to complex plasma-plasma and plasma-materials interaction, which makes the defect evolution difficult to be predicted. The theoretical model of laser ablation at this time scale is currently not complete, and the ability to control and predict nanoscale morphology is insufficient. At the ultra-high pulse repetition rate, the synergistic mechanism of multiple pulses induced heat accumulation and plasma interaction further limits the materials machining window, which requires the accurate matching of laser processing parameters with the materials characteristics. This issue can be solved by combining the real-time monitoring proposed in the challenge 1 with innovative machining strategy. The last challenge is on how to extend the processing strategy of the high-repetition-rate femtosecond laser from the laboratory to industrial applications, which requires a breakthrough in processing efficiency, cost-effectiveness and system reliability. Since the direct laser writer patterns point by point, the throughput is limited. Parallel laser micro/nano-processing is a promising method in industrial production. More than 10^5 nanostructures can be created simultaneously through laser microlens array (MLA) lithography, and the manufacturing speed is revolutionized. For example, by laser MLA lithography, ~500,000 microlenses can directly write over an area of 0.5 cm^2 within 70 s[148]. By controlling the switches of specific microlenses in MLA through liquid crystal control, the flexible direct writing of nonperiodic array can be realized, which improves the strategy applicability. In addition, the laser processing technology based on spatial light modulator (SLM) also shows flexible multifocal processing ability, but the cost is higher, which is only suitable for the parallel processing of more complex patterns.

Despite the above four main challenges, optical precision manufacturing based on femtosecond laser multiple pulses incubation is still one of the best and most promising processing methods, particularly due to its transformative applications enabled by sub-20 nm resolution and ablation efficiency enhancement in burst mode. In this review, we summarize the impact of the femtosecond laser repetition rate on multiple pulses incubation. With the increase of repetition rate, the incubation effect gradually develops from simple defect accumulation at kHz to thermal accumulation at MHz, and then to plasma interaction at GHz. The unique incubation mechanisms from kHz to GHz are also reviewed, which supports a series of micro/nano fabrication capabilities, from flexible micro/nano-structuring, nanostructure synthesis, 3D printing to efficient materials removal. The challenges and potential solutions in the research frontier and industrial applications of the femtosecond laser precision engineering based on multiple pulses incubation are also analyzed. At present, there are still many unexplained phenomena in the interaction between the femtosecond laser and materials, which needs further exploration and research. With the development of new laser sources, optical processing systems and real-time monitoring systems, the potential applications of the high-repetition-rate femtosecond laser precision engineering will be further enhanced.

References

1. Wang KY, Xing GC, Song QH et al. Micro- and nanostructured lead halide perovskites: from materials to integrations and devices. *Adv Mater* **33**, 2000306 (2021).
2. Luo XG, Tsai D, Gu M et al. Extraordinary optical fields in nanostructures: from sub-diffraction-limited optics to sensing and energy conversion. *Chem Soc Rev* **48**, 2458–2494 (2019).
3. Zhong SH, Huang ZG, Lin XX et al. High-efficiency nanostructured silicon solar cells on a large scale realized through the suppression of recombination channels. *Adv Mater* **27**, 555–561 (2015).
4. Yang J, Luo FF, Kao TS et al. Design and fabrication of broadband ultralow reflectivity black Si surfaces by laser

micro/nanoprocessing. *Light Sci Appl* **3**, e185 (2014).
5. Xu KC, Zhou R, Takei K et al. Toward flexible surface-enhanced Raman scattering (SERS) sensors for point-of-care diagnostics. *Adv Sci* **6**, 1900925 (2019).
6. Yan HP, Wang ZJ, Zhou R et al. Distribution optimization of microcone structures in the dielectric layer of a capacitive flexible pressure sensor. *Measurement* **201**, 111773 (2022).
7. Ng B, Hanham SM, Giannini V et al. Lattice resonances in antenna arrays for liquid sensing in the terahertz regime. *Opt Express* **19**, 14653–14661 (2011).
8. Fallegger F, Schiavone G, Lacour SP. Conformable hybrid systems for implantable bioelectronic interfaces. *Adv Mater* **32**, 1903904 (2020).
9. Chichkov BN, Momma C, Nolte S et al. Femtosecond, picosecond and nanosecond laser ablation of solids. *Appl Phys A* **63**, 109–115 (1996).
10. Lin ZY, Hong MH. Femtosecond laser precision engineering: from micron, submicron, to nanoscale. *Ultrafast Sci* **2021**, 9783514 (2021).
11. Yin JB, Yan HP, Dunzhu GS et al. General strategy toward laser single-step generation of multiscale anti-reflection structures by marangoni effect. *Micromachines* **13**, 1491 (2022).
12. Xu KC, Zhang CT, Zhou R et al. Hybrid micro/nano-structure formation by angular laser texturing of Si surface for surface enhanced Raman scattering. *Opt Express* **24**, 10352–10358 (2016).
13. Huang JX, Xu K, Xu SL. Super-resolution laser machining. *Int J Mach Tools Manuf* **205**, 104246 (2025).
14. Ueno K, Takabatake S, Nishijima Y et al. Nanogap-assisted surface plasmon nanolithography. *J Phys Chem Lett* **1**, 657–662 (2010).
15. Jiang QL, Chen L, Liu JK et al. Periodic transparent nanowires in ITO film fabricated via femtosecond laser direct writing. *Opto-Electron Sci* **2**, 220002 (2023).
16. Li Y, Hong MH. Parallel laser micro/nano-processing for functional device fabrication. *Laser Photonics Rev* **14**, 1900062 (2020).
17. Kawata S, Sun HB, Tanaka T et al. Finer features for functional microdevices. *Nature* **412**, 697–698 (2001).
18. Joglekar AP, Liu HH, Meyhöfer E et al. Optics at critical intensity: applications to nanomorphing. *Proc Natl Acad Sci USA* **101**, 5856–5861 (2004).
19. Lin ZY, Ji LF, Hong MH. Approximately 30 nm nanogroove formation on single crystalline silicon surface under pulsed nanosecond laser irradiation. *Nano Lett* **22**, 7005–7010 (2022).
20. Butkus S, Jukna V, Paipulas D et al. Micromachining of invar foils with GHz, MHz and kHz femtosecond burst modes. *Micromachines* **11**, 733 (2020).
21. Žemaitis A, Gaidys M, Gečys P et al. Femtosecond laser ablation by bibursts in the MHz and GHz pulse repetition rates. *Opt Express* **29**, 7641–7653 (2021).
22. Yin JB, Zhao YL, Hong MH. High performance laser induced plasma assisted ablation by GHz burst mode femtosecond pulses. *Opto-Electron Adv* **7**, 240222 (2024).
23. Lin ZY, Liu HG, Ji LF et al. Realization of ~10 nm features on semiconductor surfaces via femtosecond laser direct patterning in far field and in ambient air. *Nano Lett* **20**, 4947–4952 (2020).
24. Liu HG, Lin WX, Lin ZY et al. Self-organized periodic microholes array formation on aluminum surface via femtosecond laser ablation induced incubation effect. *Adv Funct Mater* **29**, 1903576 (2019).
25. Li ZZ, Wang L, Fan H et al. O-FIB: far-field-induced near-field breakdown for direct nanowriting in an atmospheric environment. *Light Sci Appl* **9**, 41 (2020).
26. Yin JB, Hong MH. Seed-guided high-repetition-rate femtosecond laser oxidation for functional three-dimensional silicon structure fabrication. *Opt Laser Technol* **179**, 111348 (2024).
27. Yin JB, Li YZ, Chen ZW et al. Formation of armored silicon nanowires array via high-repetition-rate femtosecond laser oxidation for robust surface-enhanced Raman scattering detection. *ACS Appl Mater Interfaces* **16**, 48667–48675 (2024).
28. Lin ZY, Liu K, Cao T et al. Microsphere femtosecond laser sub-50 nm structuring in far field via non-linear absorption. *Opto-Electron Adv* **6**, 230029 (2023).
29. Du ZR, Chen LE, Wang DC et al. 3D micro-concrete hybrid structures fabricated by femtosecond laser two-photon polymerization for biomedical and photonic applications. In *2016 IEEE International Conference on Industrial Technology (ICIT)* 1108–1114 (IEEE, 2016). http://doi.org/10.1109/ICIT.2016.7474909.
30. Kerse C, Kalaycıoğlu H, Elahi P et al. Ablation-cooled material removal with ultrafast bursts of pulses. *Nature* **537**, 84–88 (2016).
31. Kawabata S, Bai S, Obata K et al. Two-dimensional laser-induced periodic surface structures formed on crystalline silicon by GHz burst mode femtosecond laser pulses. *Int J Extrem Manuf* **5**, 015004 (2023).
32. Maiman TH. Stimulated optical radiation in ruby. *Nature* **187**, 493–494 (1960).
33. Schoonderbeek A, Biesheuvel CA, Hofstra RM et al. The influence of the pulse length on the drilling of metals with an excimer laser. *J Laser Appl* **16**, 85–91 (2004).
34. Rudd JV, Korn G, Kane S et al. Chirped-pulse amplification of 55-fs pulses at a 1-kHz repetition rate in a Ti: Al_2O_3 regenerative amplifier. *Opt Lett* **18**, 2044–2046 (1993).
35. Sugioka K, Cheng Y. Ultrafast lasers—reliable tools for advanced materials processing. *Light Sci Appl* **3**, e149 (2014).
36. Layani M, Wang XF, Magdassi S. Novel materials for 3D printing by photopolymerization. *Adv Mater* **30**, 1706344 (2018).
37. Chong TC, Hong MH, Shi LP. Laser precision engineering: from microfabrication to nanoprocessing. *Laser Photonics Rev* **4**, 123–143 (2010).
38. Gao L, Zhang QM, Gu M. Femtosecond laser micro/nano processing: from fundamental to applications. *Int J Extrem Manuf* **7**, 022010 (2025).
39. Yao YL, Chen HQ, Zhang WW. Time scale effects in laser material removal: a review. *Int J Adv Manuf Technol* **26**, 598–608 (2005).
40. Wu J, Zhou Y, Chen MX et al. Numerical modeling and simulation on nanosecond laser-target interactions. *J Phys D Appl Phys* **58**, 143004 (2025).
41. Yin JB, Yan HP, Zhou R et al. Thermal-assisted laser fabrication of broadband ultralow reflectance surface by combining marangoni flow with in situ deposition. *Nanomaterials* **13**, 480 (2023).
42. Phillips KC, Gandhi HH, Mazur E et al. Ultrafast laser processing of materials: a review. *Adv Opt Photonics* **7**, 684–712 (2015).
43. Roberts DE, du Plessis A, Botha LR. Femtosecond laser ablation of silver foil with single and double pulses. *Appl Surf Sci* **256**, 1784–1792 (2010).
44. Ashkenasi D, Lorenz M, Stoian R et al. Surface damage threshold and structuring of dielectrics using femtosecond laser pulses: the role of incubation. *Appl Surf Sci* **150**, 101–106 (1999).
45. Lin ZB, Johnson RA, Zhigilei LV. Computational study of the generation of crystal defects in a bcc metal target irradiated by short laser pulses. *Phys Rev B* **77**, 214108 (2008).
46. Paula KT, Clabel H JL, Vieira EVM et al. Femtosecond laser-induced damage threshold incubation in $SrTiO_3$ thin films. *Appl Surf Sci* **680**, 161340 (2025).
47. Mannion PT, Magee J, Coyne E et al. The effect of damage accumulation behaviour on ablation thresholds and damage morphology in ultrafast laser micro-machining of common metals in air. *Appl Surf Sci* **233**, 275–287 (2004).
48. Wang Z, Xiang ZK, Li XW et al. Dual-control of incubation effect for efficiently fabricating surface structures in fused silica.

Nanophotonics **13**, 4057–4065 (2024).
49. Wang PJ, Peng Q. Unveiling of incubation and absorption-enhanced effects occurring during multi-shot femtosecond laser ablation of aluminum and steel surfaces. *Nanotechnology* **35**, 015401 (2024).
50. Di Niso F, Gaudiuso C, Sibillano T et al. Role of heat accumulation on the incubation effect in multi-shot laser ablation of stainless steel at high repetition rates. *Opt Express* **22**, 12200 (2014).
51. Obata K, Kawabata S, Hanada Y et al. High performance micromachining of sapphire by laser induced plasma assisted ablation (LIPAA) using GHz burst mode femtosecond pulses. *Opto-Electron Sci* **3**, 230053 (2024).
52. Förster DJ, Faas S, Gröninger S et al. Shielding effects and re-deposition of material during processing of metals with bursts of ultra-short laser pulses. *Appl Surf Sci* **440**, 926–931 (2018).
53. Chen ZK, Zhou R, Hong MH. Enhanced anti-icing performance via bio-inspired papaver radicatum structuring. *J Mater Res Technol* **23**, 3811–3820 (2023).
54. Yang YY, Zhang YN, Zhang J et al. Graphene metamaterial 3D conformal coating for enhanced light harvesting. *ACS Nano* **17**, 2611–2619 (2023).
55. Yu J, Wu JG, Yang H et al. Extremely sensitive SERS sensors based on a femtosecond laser-fabricated superhydrophobic/-philic microporous platform. *ACS Appl Mater Interfaces* **14**, 43877–43885 (2022).
56. Xu J, Lan J, Li XW et al. Femtosecond laser-induced cross-periodic structures on a crystalline silicon surface under low pulse number irradiation. *Appl Surf Sci* **326**, 216–221 (2015).
57. Huang HX, Song SJ, Liu Y et al. Near-field-regulated ultrafast laser supra-wavelength structuring directly on ultrahard metallic glasses. *Adv Mater* **36**, 2405766 (2024).
58. Papadopoulos A, Skoulas E, Mimidis A et al. Biomimetic omnidirectional antireflective glass via direct ultrafast laser nanostructuring. *Adv Mater* **31**, 1901123 (2019).
59. Zhao JH, Ji PF, Lin G et al. Experimental probe into the femtosecond laser ablation thresholds in carbon fiber reinforced polymer and assessment of the measurement theories. *Polym Compos* **44**, 5232–5246 (2023).
60. Siddique RH, Gomard G, Hölscher H. The role of random nanostructures for the omnidirectional anti-reflection properties of the glasswing butterfly. *Nat Commun* **6**, 6909 (2015).
61. Morikawa J, Ryu M, Seniutinas G et al. Nanostructured antireflective and thermoisolative cicada wings. *Langmuir* **32**, 4698–4703 (2016).
62. Chen L, Cao KQ, Li YL et al. Large-area straight, regular periodic surface structures produced on fused silica by the interference of two femtosecond laser beams through cylindrical lens. *Opto-Electron Adv* **4**, 200036 (2021).
63. Zhang DS, Li XZ, Fu Y et al. Liquid vortexes and flows induced by femtosecond laser ablation in liquid governing formation of circular and crisscross LIPSS. *Opto-Electron Adv* **5**, 210066 (2022).
64. Rebollar E, Castillejo M, Ezquerra TA. Laser induced periodic surface structures on polymer films: from fundamentals to applications. *Eur Polym J* **73**, 162–174 (2015).
65. Bonse J, Gräf S. Maxwell meets marangoni-a review of theories on laser-induced periodic surface structures. *Laser Photonics Rev* **14**, 2000215 (2020).
66. Bonse J, Höhm S, Kirner SV et al. Laser-induced periodic surface structures-a scientific evergreen. *IEEE J Sel Top Quantum Electron* **23**, 9000615 (2017).
67. Rodríguez A, Morant-Miñana MC, Dias-Ponte A et al. Femtosecond laser-induced periodic surface nanostructuring of sputtered platinum thin films. *Appl Surf Sci* **351**, 135–139 (2015).
68. Déziel JL, Dumont J, Gagnon D et al. Constructive feedback for the growth of laser-induced periodic surface structures. *Phys Status Solidi C* **13**, 121–124 (2016).
69. Li C, Zhang H, Cheng GH et al. Initial cumulative effects in femtosecond pulsed laser-induced periodic surface structures on bulk metallic glasses. *J Laser Micro Nanoeng* **11**, 357–365 (2016).
70. Vo TS, Jeon B, Nguyen VPT et al. A comprehensive review of laser processing-assisted 2D functional materials and their specific applications. *Mater Today Phys* **47**, 101536 (2024).
71. Sheng YH, Wen XM, Jia BH et al. Direct laser writing on halide perovskites: from mechanisms to applications. *Light Adv Manuf* **4**, 4 (2024).
72. Zou TT, Zhao B, Xin W et al. High-speed femtosecond laser plasmonic lithography and reduction of graphene oxide for anisotropic photoresponse. *Light Sci Appl* **9**, 69 (2020).
73. Gnilitskyi I, Derrien TJY, Levy Y et al. High-speed manufacturing of highly regular femtosecond laser-induced periodic surface structures: physical origin of regularity. *Sci Rep* **7**, 8485 (2017).
74. Geng J, Yan W, Shi LP et al. Surface plasmons interference nanogratings: wafer-scale laser direct structuring in seconds. *Light Sci Appl* **11**, 189 (2022).
75. Song J, Wang HJ, Huang XX et al. In-situ study of laser-induced novel ripples formation on SiC surface by an oblique-illumination high-resolution imaging setup. *Opt Laser Technol* **169**, 110095 (2024).
76. Zhang DS, Liu RJ, Li ZG. Irregular LIPSS produced on metals by single linearly polarized femtosecond laser. *Int J Extrem Manuf* **4**, 015102 (2022).
77. Lin ZY, Ji LF, Zhou BH et al. Energy band structure perturbation induced deviation on precise ultrafast laser nano-structuring. *Mater Today Phys* **51**, 101636 (2025).
78. Geng J, Fang XG, Zhang L et al. Controllable generation of large-scale highly regular gratings on Si films. *Light Adv Manuf* **2**, 22 (2021).
79. Geng J, Shi LP, Sun XY et al. Artificial seeds-regulated femtosecond laser plasmonic nanopatterning. *Laser Photonics Rev* **16**, 2200232 (2022).
80. Cao KQ, Chen L, Wu HC et al. Large-area commercial-grating-quality subwavelength periodic ripples on silicon efficiently fabricated by gentle ablation with femtosecond laser interference via two cylindrical lenses. *Opt Laser Technol* **131**, 106441 (2020).
81. Liu JK, Jia TQ, Zhou K et al. Direct writing of 150 nm gratings and squares on ZnO crystal in water by using 800 nm femtosecond laser. *Opt Express* **22**, 32361–32370 (2014).
82. Huang M, Xu ZZ. Spontaneous scaling down of femtosecond laser-induced apertures towards the 10-nanometer level: the excitation of quasistatic surface plasmons. *Laser Photonics Rev* **8**, 633–652 (2014).
83. Li ZZ, Fan H, Wang L et al. Super-stealth dicing of transparent solids with nanometric precision. *Nat Photonics* **18**, 799–808 (2024).
84. Du ZR, Zhang CT, Li FP et al. Impact of laser-induced oxidation on silicon wafer solar cells' performance. *IEEE J Photovolt* **6**, 617–623 (2016).
85. Wang C, Tian YX, Luo Z et al. Convex grid-patterned microstructures on silicon induced by femtosecond laser assisted with chemical etching. *Opt Laser Technol* **119**, 105663 (2019).
86. Ma YC, Wang L, Guan KM et al. Silicon-based suspended structure fabricated by femtosecond laser direct writing and wet etching. *IEEE Photonics Technol Lett* **28**, 1605–1608 (2016).
87. Qiao M, Yan JF, Jiang L. Direction controllable nano-patterning of titanium by ultrafast laser for surface coloring and optical encryption. *Adv Opt Mater* **10**, 2101673 (2022).
88. Dostovalov A, Bronnikov K, Korolkov V et al. Hierarchical anti-reflective laser-induced periodic surface structures (LIPSSs) on amorphous Si films for sensing applications. *Nanoscale* **12**, 13431–13441 (2020).

89. Schnell G, Lund H, Bartling S et al. Heat accumulation during femtosecond laser treatment at high repetition rate–a morphological, chemical and crystallographic characterization of self-organized structures on Ti6Al4V. *Appl Surf Sci* **570**, 151115 (2021).
90. Shi LP, Yan J, Zhang SY et al. Burst laser-driven plasmonic photochemical nanolithography of silicon with active structural modulation. *Ultrafast Sci* **5**, 0084 (2025).
91. Öktem B, Pavlov I, Ilday S et al. Nonlinear laser lithography for indefinitely large-area nanostructuring with femtosecond pulses. *Nat Photonics* **7**, 897–901 (2013).
92. Akkilic N, Geschwindner S, Höök F. Single-molecule biosensors: recent advances and applications. *Biosens Bioelectron* **151**, 111944 (2020).
93. Arun Kumar KV, John J, Sooraj TR et al. Surface plasmon response of silver nanoparticles doped silica synthesised via sol-gel route. *Appl Surf Sci* **472**, 40–45 (2019).
94. Chinnakkannu Vijayakumar S, Venkatakrishnan K, Tan B. SERS active nanobiosensor functionalized by self-assembled 3D nickel nanonetworks for glutathione detection. *ACS Appl Mater Interfaces* **9**, 5077–5091 (2017).
95. Thakur P, Tan B, Venkatakrishnan K. Plasmon hybridisation of self-assembled 3d multiphase nano-titanium oxide towards broadband photon absorption. *Sol Energy Mater Sol Cells* **164**, 165–174 (2017).
96. Dharmalingam P, Venkatakrishnan K, Tan B. An atomic-defect enhanced Raman scattering (DERS) quantum probe for molecular level detection–Breaking the SERS barrier. *Appl Mater Today* **16**, 28–41 (2019).
97. Yan TY, Hong MH. Facile one-step synthesis of hybrid electrode based on graphitic carbon decorated by copper/copper oxide nanoparticles via laser-induced plasma processing for non-enzymatic glucose sensor. *Appl Surf Sci* **685**, 162080 (2025).
98. Liu WH, Yang J, Zhao YZ et al. Laser-ironing induced capping layer on co-ZIF-L promoting in situ surface modification to high-spin oxide–carbon hybrids on the “real catalyst” for high OER activity and stability. *Adv Mater* **36**, 2310106 (2024).
99. He XL, Datta A, Nam W et al. Sub-diffraction limited writing based on laser induced periodic surface structures (LIPSS). *Sci Rep* **6**, 35035 (2016).
100. Lin ZY, Ji LF, Hong MH. Enhancement of femtosecond laser-induced surface ablation via temporal overlapping double-pulse irradiation. *Photonics Res* **8**, 271–278 (2020).
101. Qin L, Huang YQ, Xia F et al. 5 nm nanogap electrodes and arrays by super-resolution laser lithography. *Nano Lett* **20**, 4916–4923 (2020).
102. Chen LW, Zhou Y, Li Y et al. Microsphere enhanced optical imaging and patterning: from physics to applications. *Appl Phys Rev* **6**, 021304 (2019).
103. Wang ZB, Guo W, Li L et al. Optical virtual imaging at 50 nm lateral resolution with a white-light nanoscope. *Nat Commun* **2**, 218 (2011).
104. Wu GX, Zhou Y, Hong MH. Sub-50 nm optical imaging in ambient air with 10× objective lens enabled by hyper-hemi-microsphere. *Light Sci Appl* **12**, 49 (2023).
105. Huang SY, Zhong XC, Hong MH. Optical nano-imaging via refractive index modulated microsphere compound lens. *Opt Lasers Eng* **191**, 108988 (2025).
106. Yan B, Yue LY, Monks JN et al. Superlensing plano-convex-microsphere (PCM) lens for direct laser nano-marking and beyond. *Opt Lett* **45**, 1168–1171 (2020).
107. Liu K, Lin ZY, Han B et al. Non-volatile dynamically switchable color display via chalcogenide stepwise cavity resonators. *Opto-Electron Adv* **7**, 230033 (2024).
108. Li LY, Fan XH, Xu WY et al. Bioinspired 3D-nanoprinted optical sensilla for bidirectional respiratory monitoring. *Nano Lett* **25**, 5452–5460 (2025).
109. Gissibl T, Thiele S, Herkommer A et al. Two-photon direct laser writing of ultracompact multi-lens objectives. *Nat Photonics* **10**, 554–560 (2016).
110. Keldysh LV. Ionization in the field of a strong electromagnetic wave. *J Exp Theor Phys* **20**, 1307–1314 (1965).
111. Shlomo N, Frumker E. In situ characterization of laser-induced strong field ionization phenomena. *Light Sci Appl* **14**, 166 (2025).
112. Calin BS, Popescu RC, Tanasa E et al. Laser-based 3D printing and optical characterization of optical micro-nanostructures inspired by nocturnal insects compound eyes. *Sci Rep* **15**, 3369 (2025).
113. Zhang YL, Tian Y, Wang H et al. Dual-3D femtosecond laser nanofabrication enables dynamic actuation. *ACS Nano* **13**, 4041–4048 (2019).
114. Ma ZC, Zhang YL, Han B et al. Femtosecond laser programmed artificial musculoskeletal systems. *Nat Commun* **11**, 4536 (2020).
115. Tudor A, Delaney C, Zhang HR et al. Fabrication of soft, stimulus-responsive structures with sub-micron resolution via two-photon polymerization of poly(ionic liquid)s. *Mater. Today* **21**, 807–816 (2018).
116. Kotz F, Quick AS, Risch P et al. Two-photon polymerization of nanocomposites for the fabrication of transparent fused silica glass microstructures. *Adv Mater* **33**, 2006341 (2021).
117. Meza LR, Das S, Greer JR. Strong, lightweight, and recoverable three-dimensional ceramic nanolattices. *Science* **345**, 1322–1326 (2014).
118. Blasco E, Müller J, Müller P et al. Fabrication of conductive 3D gold-containing microstructures via direct laser writing. *Adv Mater* **28**, 3592–3595 (2016).
119. Wen XW, Zhang BY, Wang WP et al. 3D-printed silica with nanoscale resolution. *Nat Mater* **20**, 1506–1511 (2021).
120. Wang YY, Yi CQ, Tian WX et al. Free-space direct nanoscale 3D printing of metals and alloys enabled by two-photon decomposition and ultrafast optical trapping. *Nat Mater* **23**, 1645–1653 (2024).
121. Bartulevicius T, Lipnickas M, Petrauskiene V et al. 30 W-average-power femtosecond NIR laser operating in a flexible GHz-burst-regime. *Opt Express* **30**, 36849–36862 (2022).
122. Bonamis G, Audouard E, Hönninger C et al. Systematic study of laser ablation with GHz bursts of femtosecond pulses. *Opt Express* **28**, 27702–27714 (2020).
123. Audouard E, Mottay E. High efficiency GHz laser processing with long bursts. *Int J Extrem Manuf* **5**, 015003 (2023).
124. Bonamis G, Mishchick K, Audouard E et al. High efficiency femtosecond laser ablation with gigahertz level bursts. *J Laser Appl* **31**, 022205 (2019).
125. Mishchik K, Bonamis G, Qiao J et al. High-efficiency femtosecond ablation of silicon with GHz repetition rate laser source. *Opt Lett* **44**, 2193–2196 (2019).
126. Park M, Gu YR, Mao XL et al. Mechanisms of ultrafast GHz burst fs laser ablation. *Sci Adv* **9**, eadf6397 (2023).
127. Žemaitis A, Gečys P, Barkauskas M et al. Highly-efficient laser ablation of copper by bursts of ultrashort tuneable (fs-ps) pulses. *Sci Rep* **9**, 12280 (2019).
128. Lopez J, Niane S, Bonamis G et al. Percussion drilling in glasses and process dynamics with femtosecond laser GHz-bursts. *Opt Express* **30**, 12533–12544 (2022).
129. Balage P, Guilberteau T, Lafargue M et al. Pump-probe imaging of ultrafast laser percussion drilling of glass in single pulse, MHz- and GHz-burst regimes. *Adv Mater Interfaces* **12**, 2400853 (2015).
130. Balage P, Bonamis G, Lafargue M et al. Advances in femtosecond laser GHz-burst drilling of glasses: influence of burst shape and duration. *Micromachines* **14**, 1158 (2023).
131. Matsumoto H, Lin ZB, Kleinert J. Ultrafast laser ablation of copper

with ~GHz bursts. *Proc SPIE* **10519**, 1051902 (2018).
132. Hirsiger T, Gafner M, Remund S et al. Machining metals and silicon with GHz bursts: surprising tremendous reduction of the specific removal rate for surface texturing applications. *Proc SPIE* **11267**, 112670T (2020).
133. Schwarz S, Rung S, Esen C et al. Enhanced ablation efficiency using GHz bursts in micromachining fused silica. *Opt Lett* **46**, 282–285 (2021).
134. Lickschat P, Metzner D, Weißmantel S. Manufacturing of high quality 3D microstructures in stainless steel with ultrashort laser pulses using different burst modes. *J Laser Appl* **33**, 042002 (2021).
135. Sakurai H, Konishi K. Laser processing of silicon with GHz burst pumped third harmonics for precise microfabrication. *Opt Express* **31**, 40748–40757 (2023).
136. Liu HG, Lin WX, Hong MH. Hybrid laser precision engineering of transparent hard materials: challenges, solutions and applications. *Light Sci Appl* **10**, 162 (2021).
137. Xu LM, Liu HG, Chua TC et al. Fabrication of SERS substrates by femtosecond LIPAA for detection of contaminants in foods. *Opt Laser Technol* **151**, 107954 (2022).
138. Hong MH, Sugioka K, Lu YF et al. Laser microfabrication of transparent hard materials and signal diagnostics. *Appl Surf Sci* **186**, 556–561 (2002).
139. Zhang J, Sugioka K, Midorikawa K. Laser-induced plasma-assisted ablation of fused quartz using the fourth harmonic of a Nd+: YAG laser. *Appl Phys A* **67**, 545–549 (1998).
140. Liu HG, Li Y, Lin WX et al. High-aspect-ratio crack-free microstructures fabrication on sapphire by femtosecond laser ablation. *Opt Laser Technol* **132**, 106472 (2020).
141. Li Y, Liu HG, Hong MH. High-quality sapphire microprocessing by dual-beam laser induced plasma assisted ablation. *Opt Express* **28**, 6242–6250 (2020).
142. Zhao YL, Yan TY, Hong MH. Enhancement of laser-induced plasma-assisted ablation of glass substrate via interacting spatial double laser pulse irradiation. *Opt Laser Technol* **180**, 111588 (2025).
143. Gaidys M, Selskis A, Gečys P et al. Stainless steel colouring using burst and Biburst mode ultrafast laser irradiation. *Opt Laser Technol* **174**, 110561 (2024).
144. Žemaitis A, Gečys P, Gedvilas M. Efficient ablation, further GHz burst polishing, and surface texturing by ultrafast laser. *Adv Eng Mater* **26**, 2302262 (2024).
145. Gaidys M, Selskis A, Gečys P et al. High-rate stainless steel laser colouring with GHz femtosecond bursts. *Opt Laser Technol* **188**, 113014 (2025).
146. Liu HG, Lin WX, Hong MH. Surface coloring by laser irradiation of solid substrates. *APL Photonics* **4**, 051101 (2019).
147. Kawabata S, Bai S, Obata K et al. Formation of two-dimensional laser-induced periodic surface structures on titanium by GHz burst mode femtosecond laser pulses. *Front Nanotechnol* **5**, 1267284 (2023).
148. Zhu YC, Zhang CQ, Hong MH. Free-form micro-lens array fabrication via laser micro-lens array lithography. *J Laser Micro Nanoeng* **19**, 67–71 (2024).

Acknowledgements

This work is supported by Human Resource Training Project of Innovation Laboratory for Sciences and Technologies of Energy Materials of Fujian Province (IKKEM) (No. HRTP-[2022]−53), National Natural Science Foundation of China (51975017), and R&D Program of Beijing Municipal Education Commission (KM202410005005).

Competing interests

Minghui Hong serves as an Executive Editor-in-Chief for the Journal, and no other author has reported any competing interests.